

Spatial changes of seismic attenuation and multiscale geological heterogeneity in the Baikal rift and surroundings from analysis of coda waves



Anna A. Dobrynina^{a,*}, Vladimir A. Sankov^{a,b}, Vladimir V. Chechel'nitsky^c, Jacques Déverchère^d

^a Institute of the Earth's Crust SB RAS, 128 Lermontov street, 664033 Irkutsk, Russia

^b Irkutsk State University, 3 Lenina Street, 664025 Irkutsk, Russia

^c Baikal Regional Seismological Center of GS RAS, 128 Lermontov street, 664033 Irkutsk, Russia

^d Institut Universitaire Européen de la Mer (IUEM), Université de Bretagne Occidentale (UBO), Domaines Océaniques – UMR 6538, Place Copernic, 29280, Plouzané, Brest, France

ARTICLE INFO

Article history:

Received 21 July 2015

Received in revised form 24 February 2016

Accepted 11 March 2016

Available online 14 March 2016

Keywords:

Baikal rift system

Quality-factor

Coda

Attenuation

Faulting

Crustal properties

ABSTRACT

The Baikal rift system is undergoing an active tectonic deformation expressed by a high level of seismic activity. This deformation leads to physical and mechanical changes of crustal properties which can be investigated by the seismic quality factor and its frequency dependence. Using a single backscattering model, a seismic quality-factor (Q_c), a frequency parameter (n) and an attenuation coefficient (δ) have been estimated by analyzing coda waves of 274 local earthquakes of the Baikal rift system for nineteen lapse time windows (W) from 10 to 100 s every 5 s and for six central frequencies (0.3, 0.75, 1.5, 3, 6 and 12 Hz). The average Q_c value increases with the frequency and lapse time window from 46 ± 52 (at 0.75 Hz) to 502 ± 109 (at 12 Hz) for $W = 10$ s and from 114 ± 49 (at 0.3 Hz) to 1865 ± 679 (at 12 Hz) for $W = 100$ s. The values of $Q_c(f)$ and δ were estimated for the whole Baikal rift system and for separate tectonic blocks: the stable Siberian Platform, main rift basins, spurs and uplifts. Along the rift system, the Q_0 -value (Q_c -factor at the frequency $f = 1$ Hz) varies within 72–109 and the frequency parameter n ranges from 0.87 to 1.22, whereas Q_0 is 134 and n is 0.48 for the stable Siberian Platform. Vertical variations of attenuation reveal that sharp changes of δ and n are confined to the velocity discontinuities. The comparison of lateral variations of seismic wave attenuation and geological and geophysical characteristics of the Baikal rift system shows that attenuation is correlated with both seismic activity and heat flow and in a lesser degree with the surface fault density and the age of the crust. Seismic wave attenuation found across the main shear zones of the south-western Baikal rift (Main Sayan strike-slip fault zone and Tunka, Obruchev and Primorsky normal faults) is increased by more than 25–60% compared to the neighboring areas.

© 2016 Elsevier B.V. All rights reserved.

1. Introduction

The attenuation of seismic waves is referred to as the decrease in the amplitude (or the energy) when the seismic wave propagates within the geological medium. Seismic wave energy decreases because of multiple scattering and intrinsic attenuation (e.g. Sato et al., 2012 and references therein). Seismic wave scattering reflects elastic properties of the medium and is produced by irregular topography, complex surface geology, faults and cracks and other small-scale heterogeneities of crustal or mantle rocks. These heterogeneities generally decrease with depth and are hardly resolved by conventional tomographic methods. Conversely, absorption depends on anelastic properties of the medium such as viscous dissipation or fluid flow within the fault network (Mavko et al., 2009; Sato et al., 2012). In order to describe the seismic

wave attenuation, a non-dimensional parameter Q (quality factor) is commonly used, which is defined as the ratio of the wave energy to the energy dissipated per cycle of oscillation (Knopoff and Hudson, 1964; Aki and Chouet, 1975).

Several methods of Q -factor determination were developed, based either on active or on passive seismic experiments. In the latter case, the seismic Q -factor may be obtained for direct P -(Q_p), S -(Q_s) or coda waves (Q_c). Coda wave analysis is the widely used method (see e.g. Aki and Chouet, 1975; Rautian and Khalturin, 1978; Singh and Herrmann, 1983; Pulli, 1984; Gusev, 1995; Sato et al., 2012; Mak et al., 2004; Ma'hood and Hamzehloo, 2009; Dobrynina, 2011; Kopnichev and Sokolova, 2012). Aki (1969) and Aki and Chouet (1975) were among the first ones to have determined the seismic quality factor using coda waves. For explaining the coda wave pattern, Aki suggested a single backscattering model which explains the coda waves as a superposition of secondary waves reflected by the heterogeneities randomly distributed in the crust and the upper mantle (Aki, 1969; Aki and Chouet, 1975; Rautian and Khalturin, 1978). Seismic wave attenuation

* Corresponding author at: 664033, off. 224G, 128, Lermontov street, Irkutsk, Russia.
E-mail address: dobrynina@crust.irk.ru (A.A. Dobrynina).

is strongly dependent on the frequency; this dependence is typically described by a power law (Mitchell, 1981):

$$Q_c(f) = Q_0 \cdot \left(\frac{f}{f_0}\right)^n, \quad (1)$$

where Q_c is the quality-factor for the coda waves, Q_0 is the Q_c value at the reference frequency f_0 (usually $f_0 = 1$ Hz), and n is the frequency parameter, which varies from place to place depending on the heterogeneity of the medium (Aki and Chouet, 1975). The Q_c and n values are assumed to partly reflect the tectonic activity of the corresponding region: indeed, for tectonically active regions, Q_c decreases in the frequency range 0.1–25 Hz (Aki, 1982) and has a strong dependence on n -value in the frequency range 1.5–25 Hz (Aki and Chouet, 1975).

Since the development of dense seismic arrays in the 90's, coda wave analyses at high frequencies have been used to quantify the spatial changes of absorption and scattering properties of the continents, leading to a better understanding of the origin of attenuation (e.g. Calvet et al., 2013; Mayor et al., 2014, and references therein). The comparison of attenuation parameters for different tectonic settings has shown that (1) active tectonic areas are characterized by low Q_c -values ($Q_c < 200$) and high n -values ($n > 0.8$), (2) stable tectonic regions are characterized by high Q_c -values ($Q_c > 600$) and low n -values (< 0.5), and (3) Q_c -values for areas with moderate tectonic activity vary within these values (Sato and Fehler, 1998; Mak et al., 2004).

In this work, the seismic quality-factors (Q_s and Q_c), their frequency dependence (n) and the attenuation coefficient (δ) are studied by analyzing the body S - and coda waves of local earthquakes of the Baikal rift system (BRS, Fig. 1). Not many studies of quality factor have been

done in the Baikal rift system: the Q -factor is known only for some local areas of the Baikal rift system. Earlier, using the method of the predominant periods, the Q_s value was obtained for the Olkhon island ($Q_s = 1000$ – 2000), the Barguzin, Muya and Chara basins ($Q_c = 140$ – 700 , periods $T = 0.6$ – 1.7 s), the south-western part of BRS ($Q_c = 150$), and qualitative map of the coda wave attenuation in the upper mantle was estimated (Dobrynina, 2011, and references therein). Values of the quality-factor from direct P - and S -waves were obtained using local, temporary seismic networks for some local areas such as the central part of the Baikal rift ($Q_s = 400$ and $Q_s = 1400$ for frequencies $f = 2$ and 8 Hz), the Barguzin ($Q_p = 500$, $Q_s = 400$) and the North-Muya ($Q_s = 250$) regions (Dobrynina, 2011 and references therein). Finally, an active seismic experiment has provided attenuation parameters of P - and S -waves for the crust and the upper mantle of the Siberian Platform ($Q_p = 168$, $Q_s = 340$, $f = 1$ – 6 Hz, epicentral distances $\Delta = 18$ – 181 km, $Q_p = 154$, $Q_s = 508$, $f = 1$ – 8 Hz, $\Delta = 9$ – 148 km) and the quality-factor for P -waves propagating along ($Q_p = 157$) and across ($Q_p = 82$) the active faults of the Transbaikalian area (Dobrynina, 2011, and references therein). Attenuation parameters were also approximated for the SW Baikal rift system and for the whole rift system on the basis of a limited data set (Dobrynina, 2011; Dobrynina et al., 2011). However, the use of different methods for attenuation parameter determination results into some important discrepancies or inaccuracies. Actually, there have been no data on the quality-factor for the whole Baikal rift system until now.

Values of seismic quality factor, frequency parameter, attenuation coefficient and their variations with depth have also been obtained worldwide, for instance in the southern part of the Kenya rift and in the northern Basin and Range Province (Dobrynina et al., 2012;

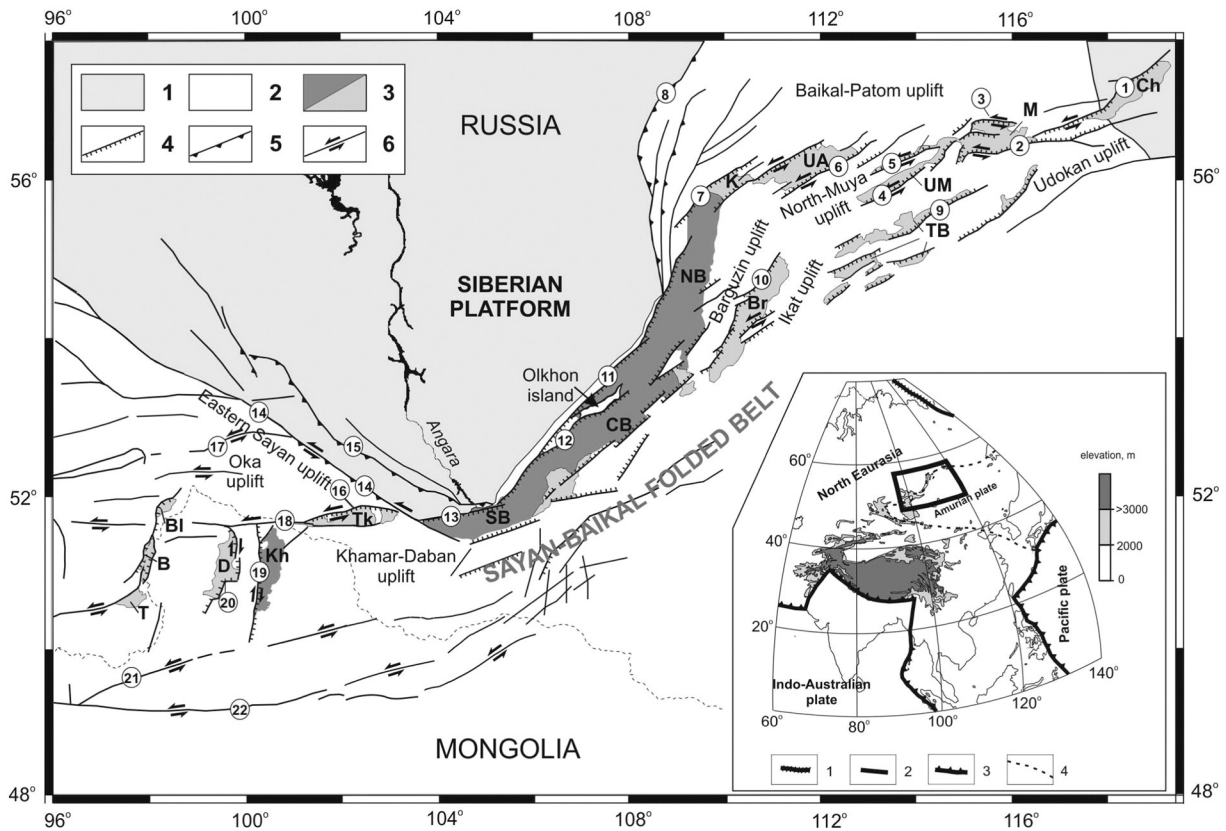


Fig. 1. Neotectonic scheme of the Baikal rift system and surroundings. 1 – Siberian platform; 2 – Sayan-Baikal folded area; 3 – Cenozoic rift basins: Ch – Chara, M – Muya, UM – Upper Muya; TB – Tsipa-Baunt; UA – Upper Angara; K – Kitchera; NB – North Baikal; Br – Barguzin; CB – Central Baikal; SB – South Baikal; Tk – Tunka; Kh – Khubsugul; D – Darkhat; BI – Belinskaya; B – Busingol; T – Terekhol; 4–6 – faults: 4 – normal; 5 – thrust and reverse; 6 – strike-slip. Numbers within circles denote main faults: 1 – Kodar; 2 – South-Muya; 3 – North-Muya; 4 – Upper Muya; 5 – Muyakansky; 6 – Upper Angara; 7 – Kitchera; 8 – Akitkan; 9 – Tsipa-Baunt; 10 – Barguzin; 11 – Primorsky; 12 – Morsky; 13 – Obruchev; 14 – Main Sayan Fault; 15 – Peredovoy; 16 – Tunka; 17 – Okino-Zhombolok; 18 – Baikal-Mondy; 19 – Khubsugul; 20 – Darkhat; 21 – Tsetserleg; 22 – Bolnai (Khangai). Inset locates the study region within Asia: 1 – study zone; 2 – mains strike-slip faults; 3 – subduction zones; and 4 – Amurian plate boundary.

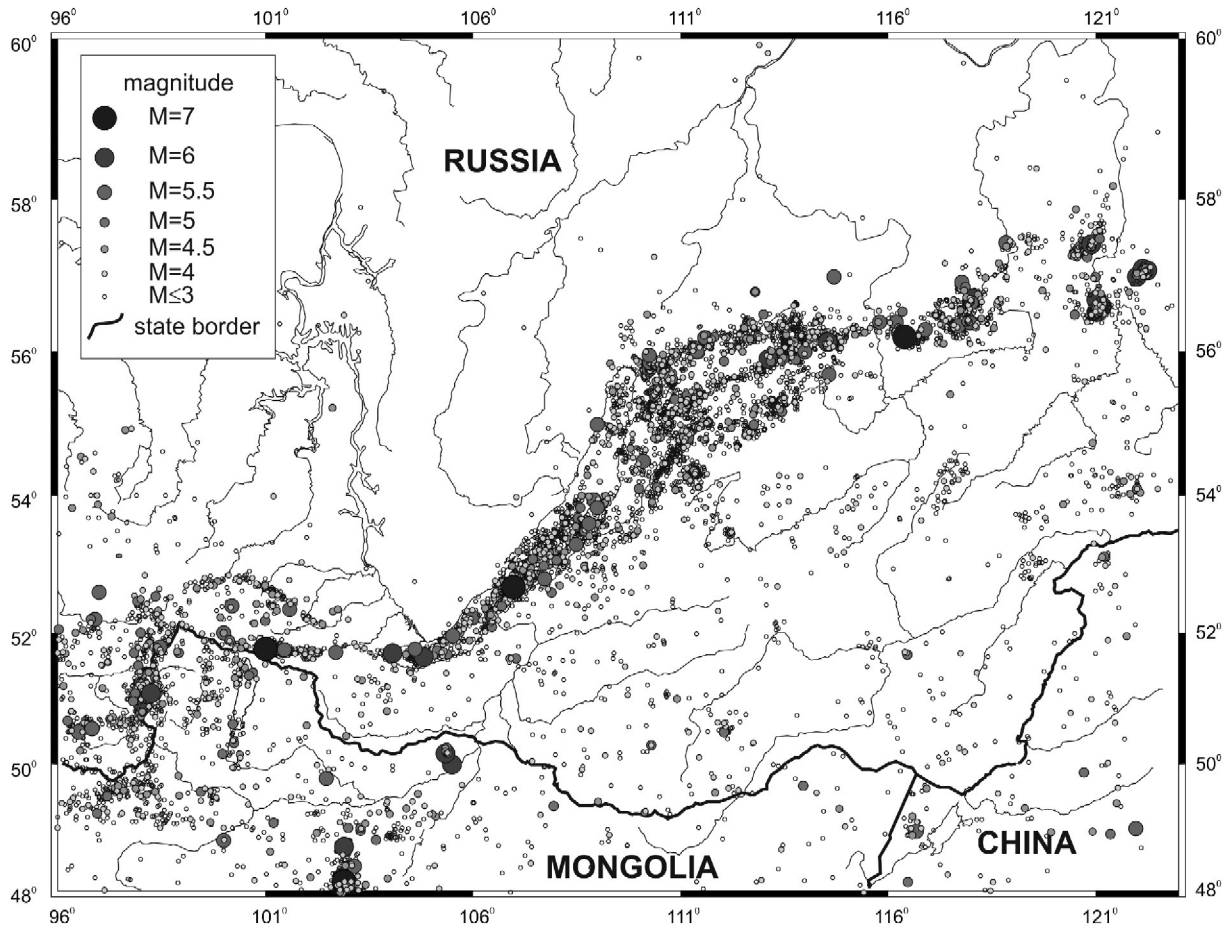


Fig. 2. Seismicity of the Baikal rift system in the span time 1950–2012. (data base from Baikal Regional Seismological Center, Geophysical Survey of the Russian Academy of Sciences).

Dobrynina, 2013). The main aims of the present study are to determine with as much accuracy as possible the seismic wave attenuation pattern in the crust and upper mantle of the Baikal rift system and to perform comparisons with those found in other rift zones.

2. Tectonic setting, deep structure and seismicity

2.1. Geological domains, faults and main structures

The Baikal rift system (Fig. 1) stretches along the edge of the Siberian Platform and through the mountain structures of East Siberia to South Yakutia (Logatchev and Florensov, 1978). The first order tectonic structures of the region are the Archaean–Proterozoic–Siberian Platform and Sayan–Baikal folded belt (Fig. 1). The Sayan–Baikal folded belt includes a number of tectonic terrains with ages varying from Low Proterozoic to Low Paleozoic times.

The South Baikal basin is the "historical" core of the Baikal rift system (Logatchev, 1993). It is confined to the boundary of the Siberian Platform with the Transbaikal belt and hosts the longest and the deepest basin of the Baikal rift system born at the transition between Cretaceous and Paleogene. During Oligocene and Miocene times, the rifting has propagated from the South Baikal basin toward the SW and NE by the formation of a series of basins (Fig. 1). The rift system is contiguous with the Siberian Platform in its middle part only. On both ends, it is separated from the platform by transition structures, namely the Sayan and Baikal–Patom uplifts (Fig. 1).

The rift grabens and half-grabens are bordered by active normal faults. The displacement amplitudes of the major normal faults reach

1500–2000 m (Logatchev and Florensov, 1978; San'kov et al., 2000), while some limited horizontal displacements are reported on the wings of the Baikal rift system (e.g. San'kov et al., 2000; Jolivet et al., 2013). Faults with sub-latitudinal and sub-meridional strikes depict left-lateral and right-lateral strike-slip components, respectively.

2.2. Strain and stress field, heat flow and velocity anomalies of the mantle

Microstructural studies (Sherman and Dneprovsky, 1989; Delvaux et al., 1997; San'kov et al., 1997), GPS measurements (Calais et al., 2003; San'kov et al., 2009), earthquake focal mechanisms and seismotectonic analyses (Petit et al., 1996; Solonenko et al., 1997; Melnikova and Radziminovich, 2007) all indicate that in the center of the rift system, extensional regime dominates. Conversely, the rift tips depict a dominant strike-slip type of tectonic stresses, whereas oblique extension characterizes the northeastern part of the rift system.

The Siberian Platform and the NE rift system are characterized by low to moderate heat flow (15–64 mW/m²), except locally, near the edge of the Platform or in the Muya region (Golubev, 2000, 2007; Lysak, 2002). Heat flow ranges from 28 to 106 mW/m² in the Sayan–Baikal folded area and gets higher (53–152 mW/m²) in the Barguzin region (see Section 5 Part). The highest local anomaly of heat flow is found in the Khubsugul basin (up to 500 mW/m²). The Baikal basin as a whole is characterized by a very irregular heat flow distribution ranging from 18 to 474 mW/m². It should be noted that the highest values are confined to the main fault zones and are assumed to reflect the influence of a convective component of heat flow (Golubev, 2000, 2007).

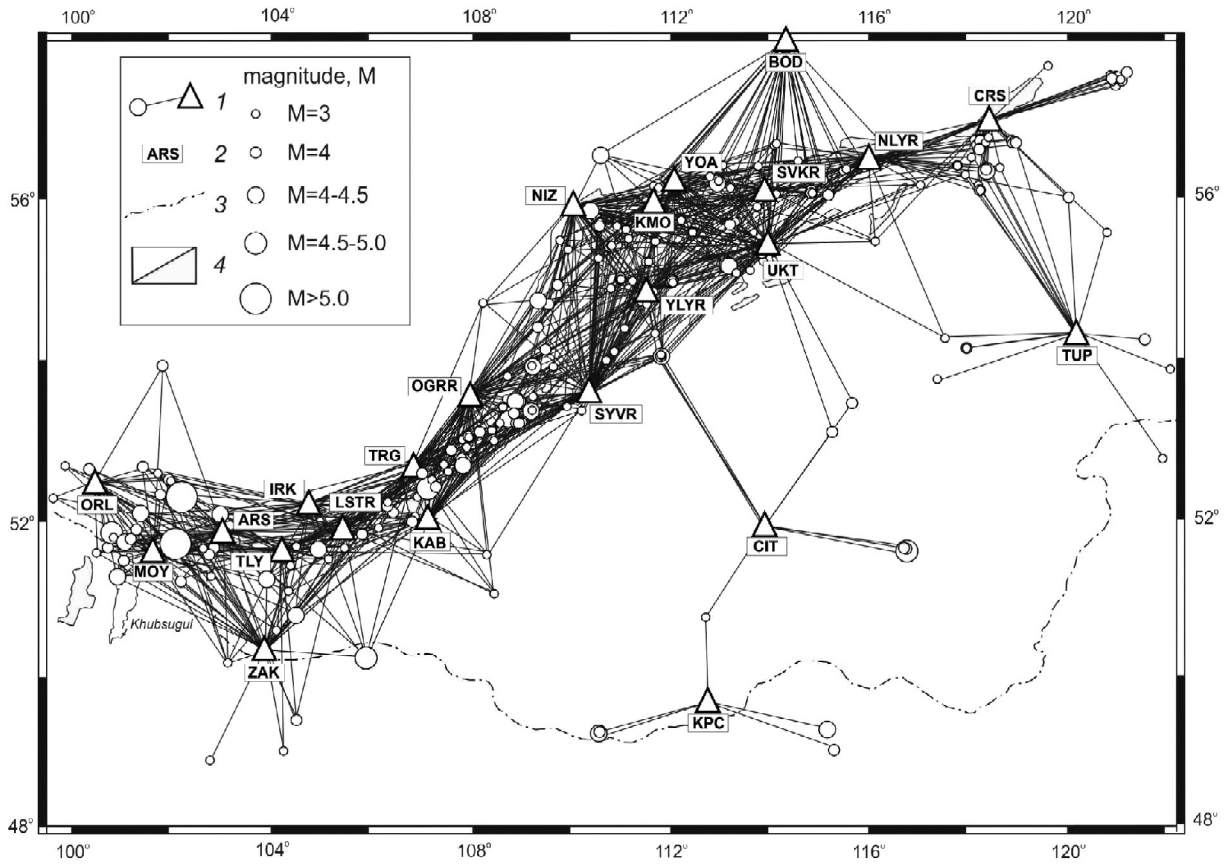


Fig. 3. Map of the spatial covering of the study area by 'source-receiver' seismic paths (i.e. paths from source to receiver): 1 – seismic stations; 2 – international code of the seismic station; 3 – state border; and 4 – Cenozoic rift basins.

Velocity studies of the crust and the upper mantle by deep seismic sounding have revealed a low velocity layer in the upper part of the crust of the Baikal rift (Krylov et al., 1981). Its position agrees with other

data sets such as seismology, magnetometry and magneto-telluric sounding and is found all along the rift system (Krylov et al., 1981). Previously, Rogozhina and Kozhevnikov (1979) have inferred a large low velocity

Table 1
Seismic stations of the Baikal rift system.

Station/international code	Coordinates, degrees		h, m	Type	f, Hz	N	Δ_{min} , km	Δ_{max} , km	$\Delta_{mean} \pm sd$, km
	N°	E°							
1	2	3	4	5	6	7	8	9	10
Arshan/ARS	51.920	102.423	970	B-11	0.5–20	144	27	349	190 ± 95
Bodaibo/BOD	57.819	114.004	245	B-11	0.5–10	15	131	321	207 ± 85
Chara/CRS	56.900	118.269	700	B-11	0.5–20	144	21	176	73 ± 50
Chita/CIT	52.021	113.552	790	B-11	0.5–20	15	160	208	195 ± 20
Irkutsk/IRK	52.243	104.271	467	B-10	0.5–10	183	62	361	209 ± 73
Kabansk/KAB	52.050	106.654	468	B-10	0.5–10	150	20	525	274 ± 164
Khapcheranga/KPC	49.704	112.379	953	B-11	0.5–20	15	123	202	169 ± 29
Kumora/KMO	55.887	111.201	480	B-11	0.5–20	150	43	495	307 ± 75
Listvyanka/LSTR	51.868	104.832	450	B-11	0.5–20	159	20	404	216 ± 95
Mondy/MOY	51.667	100.993	1303	B-11	0.5–20	183	15	451	188 ± 155
Nelyaty/NLYR	56.491	115.703	596	B-11	0.5–20	27	15	109	58 ± 32
Nizhneangarsk/NIZ	55.775	109.541	487	B-10	0.5–10	84	30	226	96 ± 68
Ongureny/OGRR	53.643	107.595	495	B-11	0.5–20	105	42	236	92 ± 50
Orlik/ORL	52.539	99.810	1360	B-11	0.5–20	183	20	512	256 ± 169
Severomuysk/SVKR	56.117	113.559	850	B-10	0.5–10	45	20	69	47 ± 16
Suvo/SYVR	53.658	109.999	490	B-11	0.5–20	45	27	161	105 ± 43
Talaya/TLY	51.681	103.644	579	B-11	0.5–20	224	21	329	200 ± 77
Tupik/TUP	54.425	119.954	650	B-11	0.5–20	63	91	270	212 ± 55
Tyrgan/TRG	52.760	106.348	718	B-11	0.5–20	279	21	501	223 ± 144
Uakit/UKT	55.489	113.627	1140	B-11	0.5–20	27	2	77	39 ± 26
Ulyunhan/YLYR	54.876	111.162	560	B-11	0.5–20	96	5	187	61 ± 48
Uoyan/YOA	56.133	111.724	500	B-10	0.5–10	42	23	62	40 ± 14
Zakamensk/ZAK	50.382	103.281	1200	B-11	0.5–20	201	32	674	257 ± 112

Caption: 1 – station's name and international code; 2, 3 – coordinates (latitude and longitude), 4 – elevation, 5 – type of receiver: B-10 is a Baikal-10, B-11 is a Baikal-11 (details in the text), 6 – working frequency band in Hz, 7 – Number of waveforms used in each station (taking into account all three components), and 8–10 – minimum, maximum and mean distances of seismic events, respectively, with corresponding standard deviation.

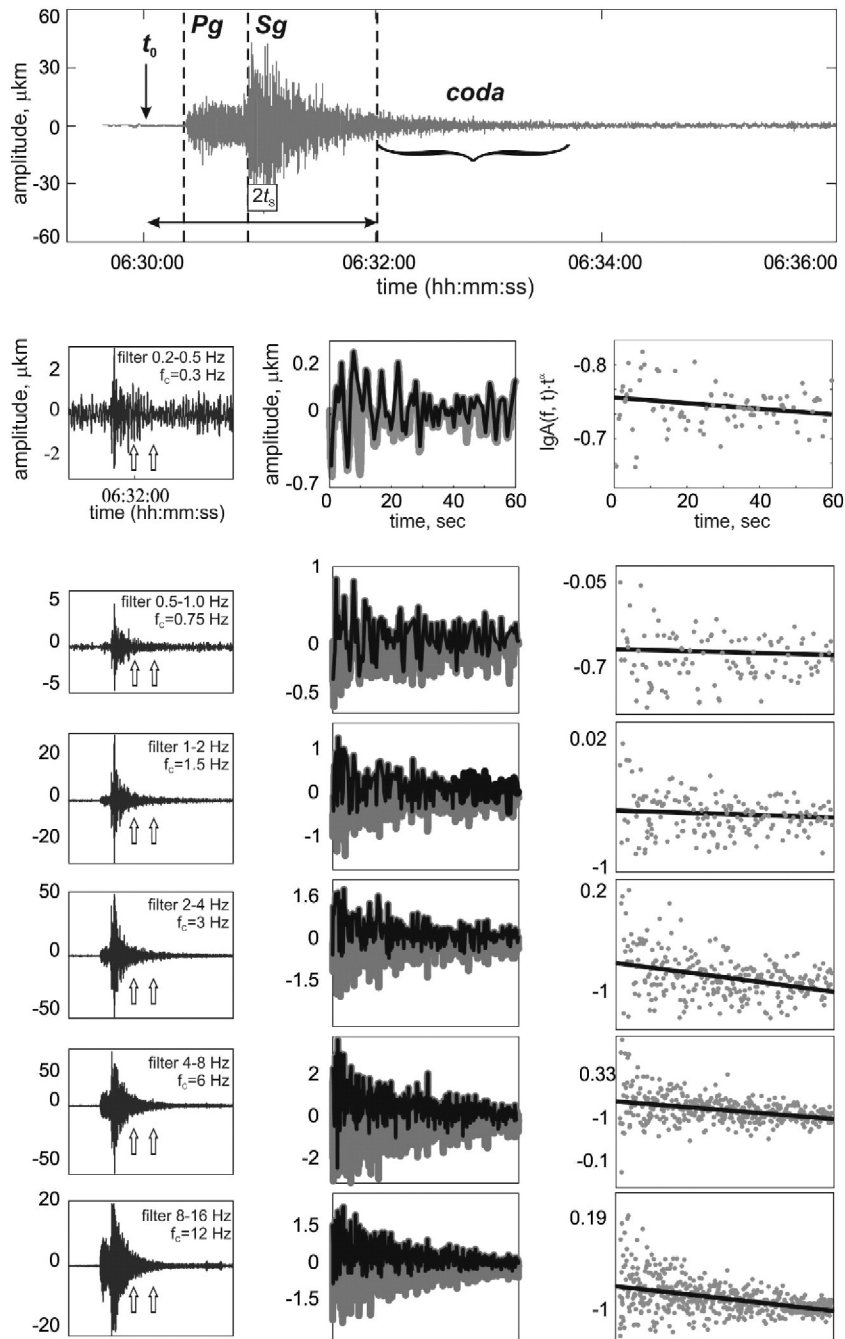


Fig. 4. An example of coda processing for Q_c calculations. Top: original (non-filtered) seismogram. Arrow shows the origin time of the event, bracket the analyzed part of the coda. Bottom left: filtered seismograms (frequency bands 0.2–0.5, 0.5–1.0, 1.0–2.0, 2.0–4.0, 4.0–8.0 and 8.0–16.0 Hz, respectively). Middle: filtered coda segments selected to compute Q_c (lapse time window of 60 s); the filtered seismogram is shown in gray, the envelope based on peak amplitudes is shown in black. Right: amplitudes of coda-wave versus time and corresponding regression lines obtained by least square method.

mantle anomaly below the Sayan-Baikal and Transbaikal belts, later on imaged by teleseismic tomography (Gao et al., 1994; Zorin et al., 2002), which was assumed to begin immediately under the bottom of the crust of the Baikal rift and to plunge down to 120 km under the edge of the Siberian Platform. Further studies using gravimetrical and seismological data instead indicate a minimum lithospheric thickness of 70 km under the southern part of the Baikal depression (Tiberi et al., 2003) and no significant lithosphere thinning under most part of the Baikal basin (Anan'in et al., 2009; Mordvinova and Artemyev, 2010). Inverse models of gravity data (Petit and Déverchère, 2006) show that the area of lithosphere thinning in the central part of the Baikal rift system is significantly displaced to the east relative to the Baikal depression.

2.3. Crustal thickness changes

Results of magneto-telluric sounding show that the roof of the layer with high electrical conductivity identified within the mantle lies at 200 km depth under the Platform, at 100 km depth under the southern Baikal rift and at 60 km depth in the northern rift (Popov, 1990; Zorin et al., 2002). Deep sounding data (Mats et al., 2001) and gravity analyses (Petit et al., 1997) show that the crustal thickness varies within 35–57 km under the South Baikal basin, 40–42 km under the North Baikal basin, 43–55 km under uplifts of for the NE part of the rift system, 43–55 km under uplifts of for the SW part of the rift and 37–43 km under the Siberian Platform. New deep seismic sounding data (Suvorov et al.,

Table 2
Earthquakes used for Q_s -values estimation.

Date dd.mm.yyyy	Origin time	M_L	Coordinates, degrees		Seismic stations
			N°	E°	
1	2	3	4	5	6
24.05.2003	21–49	4.5	55.01	110.68	KMO, NIZ, SYVR, YLYR, YOA
16.09.2003	11–24	5.2	56.05	111.34	KMO, NIZ, SVKR, UKT, YLYR, YOA
17.09.2003	02–59	4.9	51.75	101.46	ARS, MOY, ORL, TLY
01.12.2003	20–55	4.4	56.06	111.31	KMO, NIZ, SVKR, UKT, YLYR, YOA
19.01.2004	23–50	4.5	51.89	100.15	ARS, MOY, ORL
28.06.2004	14–22	4.8	56.68	117.97	CRS, NLYR
02.01.2005	00–24	4.9	56.66	118.01	CRS, NLYR
23.02.2005	19–55	4.6	52.35	101.59	ARS
10.11.2005	19–29	5.9	57.37	120.77	CRS
11.12.2005	15–54	5.4	57.43	120.9	CRS
14.12.2005	23–12	4.4	57.46	120.88	CRS
26.01.2006	16–57	4.6	57.4	120.9	CRS
08.02.2006	15–31	4.4	55.35	110.87	KMO, NIZ, YLYR, YOA
19.05.2006	22–54	4.3	57.45	120.87	CRS
04.12.2006	09–14	4.7	55.68	110.16	KMO, NIZ, YLYR, YOA
11.12.2006	09–08	4.6	55.69	110.18	KMO, NIZ, YLYR, YOA

Comment: 1, 2 – date and origin time of event, 3 – local magnitude, 4, 5 – coordinates (latitude and longitude), and 6 – seismic stations whose records are used to calculate the Q_s -values.

2002) do not detect any thinning of the crust under the rift basin. According to Thybo and Nielsen (2009), the presence of basalt intrusions explains the flat Moho and conceals the expected crustal thinning under the Baikal rift system.

2.4. Seismicity pattern

The Baikal rift system is characterized by a high level of seismic activity (Fig. 2). Since 1950, thirteen earthquakes with magnitude $M_s \geq 6$ occurred here, while magnitudes up to 8.2 is assumed according to historical data (Kondorskaya and Shebalin, 1977). The number of weak and moderate events (with magnitude $M_L \geq 1.4$) is fairly large – about 3–4 thousands earthquakes per year (Radziminovich et al., 2013). The epicenters form extensive belts along strike of the rift structures (Fig. 2). Most earthquakes in the southern part of the Baikal rift system (South Baikal and Tunka basins) occur at depths of 10–25 km (Radziminovich, 2010, and references therein). According to data from local seismic station networks, the hypocenters of the South and Central Baikal Lake are located at depths of 9–21 km with maximum peak in the range 14–19 km (Suvorov and Tubanov, 2008). The deepest earthquakes are located in the lower crust and in the upper mantle at depths of 32–46 km (Déverchère et al., 1991).

3. Data and methods used

The waveform data used in the present work were obtained by a permanent regional network (local code is BYKL, the FDSN network code – BY) of digital seismic stations from the Baikal regional seismological center of the Geophysical Survey of the Russian Academy of Sciences (RAS). The network consists of 23 stations, nineteen of which are located directly within the rift system (Fig. 3).

The stations are equipped with the digital seismic instrumentation of the “Baikal-10, 11” type, developed at the Geological Survey of the Siberian Branch of RAS (Table 1). The equipment set has three single

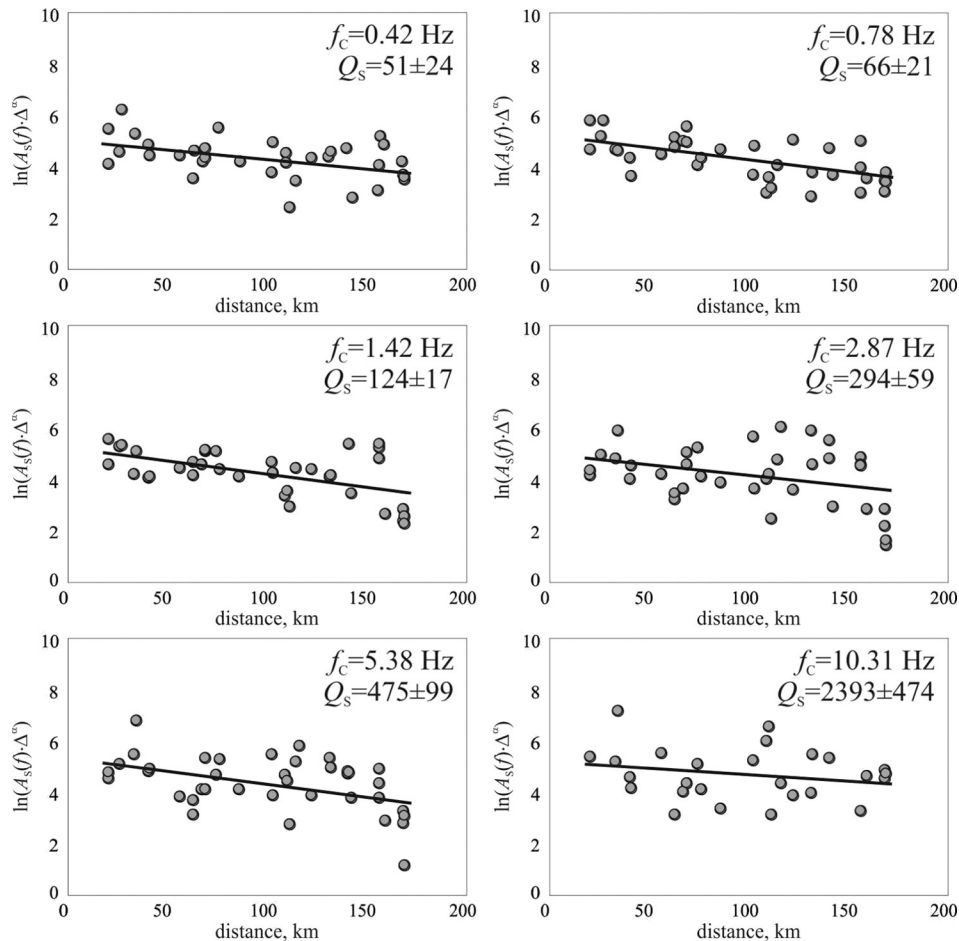


Fig. 5. An example of Q_s -values calculation for different frequency ranges (for each frequency range, Q_s -value and central frequency are shown).

Table 3
Quality-factor Q_c at different central frequencies f and for different lapse time windows W .

W , sec	$f = 0.3$ (0.1–0.5)		$f = 0.75$ (0.5–1.0)		$f = 1.5$ (1.0–2.0)		$f = 3.0$ (2.0–4.0)		$f = 6.0$ (4.0–8.0)		$f = 12.0$ (8.0–16.0)		N
	$Q_c \pm \sigma$	N	$Q_c \pm \sigma$	N	$Q_c \pm \sigma$	N	$Q_c \pm \sigma$	N	$Q_c \pm \sigma$	N	$Q_c \pm \sigma$	N	
10	–	–	46 ± 52	500	65 ± 34	387	127 ± 49	252	263 ± 67	121	502 ± 109	75	1335
15	–	–	52 ± 36	490	95 ± 41	361	195 ± 61	241	375 ± 86	142	725 ± 137	141	1375
20	43 ± 48	255	62 ± 37	428	123 ± 50	363	249 ± 69	251	494 ± 103	199	944 ± 178	239	1735
25	45 ± 37	257	74 ± 38	405	145 ± 51	339	299 ± 76	283	593 ± 123	252	1098 ± 201	373	1909
30	48 ± 37	261	83 ± 37	395	174 ± 61	347	350 ± 93	313	703 ± 143	331	1227 ± 223	469	2116
35	50 ± 32	272	99 ± 44	380	196 ± 67	355	397 ± 105	337	788 ± 159	386	1336 ± 281	538	2268
40	54 ± 32	276	110 ± 45	399	214 ± 70	374	449 ± 117	370	879 ± 183	472	1429 ± 333	573	2464
45	57 ± 30	254	119 ± 47	408	231 ± 75	388	493 ± 124	419	959 ± 208	554	1492 ± 374	586	2609
50	67 ± 40	256	127 ± 47	425	252 ± 80	410	535 ± 135	434	1014 ± 224	607	1557 ± 413	583	2715
55	67 ± 31	237	138 ± 53	437	282 ± 94	437	582 ± 144	463	1073 ± 249	652	1590 ± 430	560	2786
60	76 ± 38	242	150 ± 57	440	305 ± 105	428	629 ± 153	502	1128 ± 271	701	1626 ± 462	548	2861
65	82 ± 44	230	157 ± 59	442	324 ± 106	438	682 ± 175	534	1177 ± 295	730	1681 ± 504	532	2906
70	90 ± 50	223	168 ± 62	448	349 ± 114	456	722 ± 169	578	1208 ± 308	742	1716 ± 521	515	2962
75	91 ± 44	209	180 ± 66	457	369 ± 120	441	763 ± 179	605	1242 ± 325	740	1745 ± 549	494	2946
80	97 ± 49	204	189 ± 65	461	401 ± 132	468	805 ± 188	641	1261 ± 330	742	1767 ± 560	474	2990
85	99 ± 43	203	199 ± 70	449	420 ± 135	474	845 ± 196	681	1279 ± 341	731	1790 ± 592	446	2984
90	105 ± 44	204	209 ± 75	450	450 ± 143	492	875 ± 201	695	1289 ± 343	710	1836 ± 661	414	2965
95	111 ± 48	201	222 ± 81	446	474 ± 143	508	910 ± 215	734	1289 ± 330	685	1835 ± 673	379	2953
100	114 ± 49	201	232 ± 86	421	505 ± 151	534	933 ± 218	759	1301 ± 345	672	1865 ± 679	348	2935

Comment: in parentheses frequency ranges are shown (in Hz); σ – root mean square and N – quantity of individual measurements of Q -factor at respective central frequency.

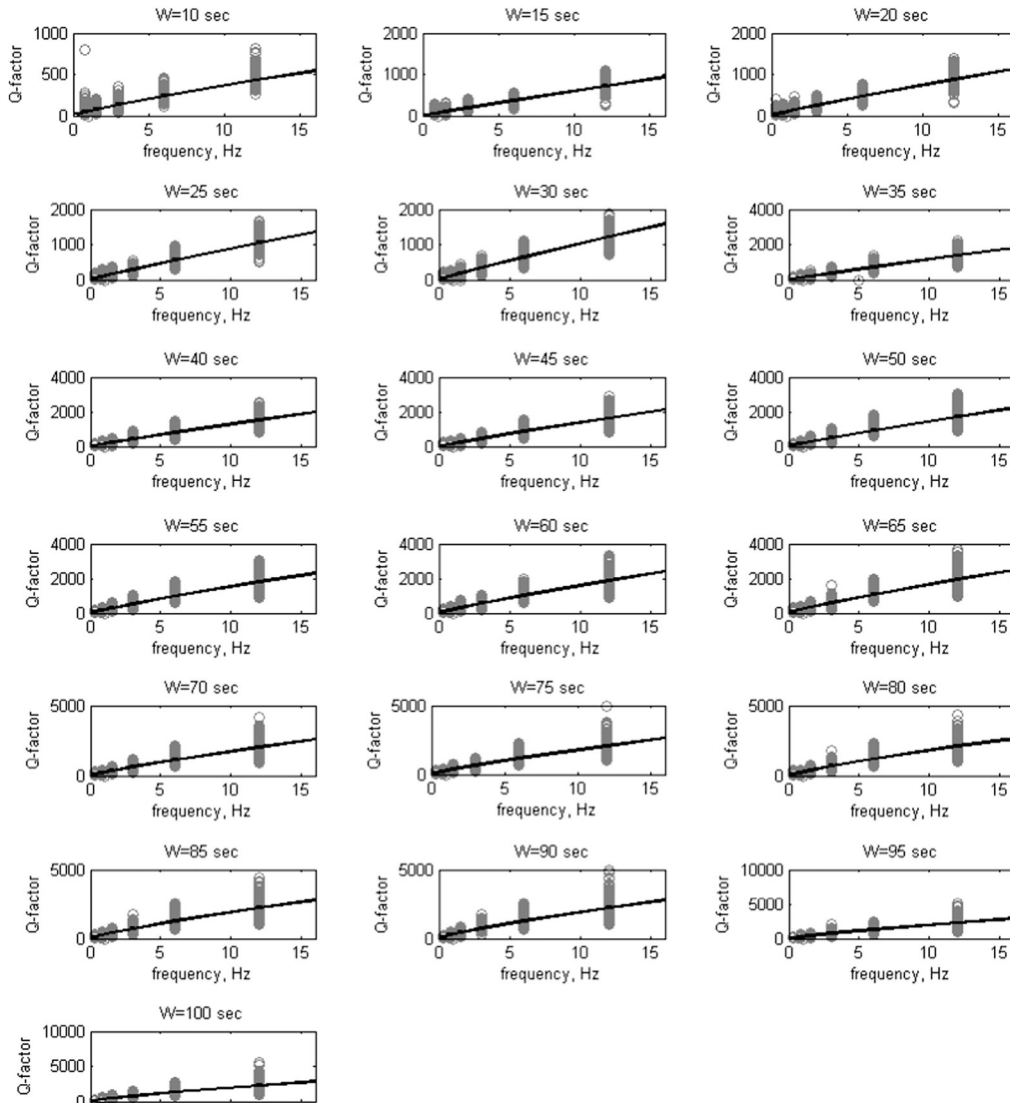


Fig. 6. Quality factor versus frequency for various coda window lengths (a). Circles show individual values of the quality factor for an individual earthquake at the appropriate central frequency, and black line shows the empirical curve according to relation (1). See text for details.

Table 4The variations of the attenuation parameters (Q_0 , n , δ) with the lapse time window.

W , sec	Q_0	σ_{Q_0}	n	σ_n	δ , km^{-1}	σ_δ , km^{-1}
1	2	3	4	5	6	7
10	53	4	0.84	0.07	0.0167	0.0018
15	67	7	0.95	0.02	0.0132	0.0020
20	95	8	0.89	0.06	0.0093	0.0011
25	109	7	0.91	0.04	0.0081	0.0007
30	124	7	0.92	0.04	0.0071	0.0006
35	140	5	0.92	0.02	0.0063	0.0003
40	155	7	0.92	0.03	0.0057	0.0004
45	166	9	0.92	0.03	0.0053	0.0004
50	183	11	0.9	0.04	0.0048	0.0004
55	196	13	0.89	0.04	0.0045	0.0004
60	215	15	0.87	0.04	0.0041	0.0004
65	229	18	0.86	0.05	0.0039	0.0004
70	246	20	0.85	0.05	0.0036	0.0004
75	258	22	0.84	0.05	0.0034	0.0004
80	275	25	0.82	0.06	0.0032	0.0004
85	288	27	0.82	0.06	0.0031	0.0004
90	303	28	0.8	0.06	0.0029	0.0004
95	320	31	0.79	0.07	0.0028	0.0004
100	335	33	0.77	0.07	0.0026	0.0004

Comment: 1 – lapse time window (in sec), 2, 3 – the quality factor at the reference frequency $f_0 = 1$ Hz and its standard deviation, 4, 5 – the frequency parameter and its standard deviation, 6, 7 – the attenuation coefficient at the frequency 1 Hz and its standard deviation. The attenuation coefficient δ is determined from the Q_C -values using the relation: $\delta = \pi \cdot f / (V_C \cdot Q_C)$, where V_C – the coda-wave velocity.

component short-period seismometers (SM-3, SM-3KV) with the seismometer gain are 20 and ~ 200 V/m/s, which record the velocity from 0.01–1000 $\mu\text{m/s}$, and three channels of low sensitivity (seismometers OSP-2M) for recording the acceleration from 50 to 500 $\mu\text{m/s}^2$ up to 100–250 cm/s^2 . The sampling frequency is 100 samples per second. The seismic stations of 'Baikal-10' and 'Baikal-11' types differ in bandwidth: the response curves have enough narrow flat area – from 0.5 Hz to 10 Hz for 'Baikal-10' and up to 20 Hz for 'Baikal-11' (see Table 1).

In order to estimate the attenuation parameters, we used two methods: a single back-scattering model for the coda wave (Aki and Chouet, 1975) and a method of maximum amplitudes for direct shear waves (Bath, 1974). The Q_C -values are calculated through the *CodaQ* subroutine of *Seisan* (Havskov and Ottemoller, 2003) and Q_S -values are calculated through our own software realized in the Matlab environment.

According to Aki and Chouet (1975), the amplitude of the coda wave A at lapse time t seconds from the origin time for a bandpass-filtered seismogram at the central frequency f is related to the attenuation parameter Q_C by the following equation:

$$A(f, t) = S(f) \cdot t^{-\alpha} \cdot e^{-\frac{\pi f t}{2 Q_C}}, \quad (2)$$

where $S(f)$ is the coda wave source factor at frequency f , α is the geometrical spreading parameter. The single backscattering model assumes that the coda waves are a superposition of scattered S-waves reflected by the heterogeneities randomly distributed in the crust and the upper mantle (Aki, 1969; Aki and Chouet, 1975; Rautian and Khalturin, 1978). If the coda is considered to be composed of scattered S-waves then the geometrical spreading exponent for body waves is assumed ($\alpha = 1$, Sato and Fehler (1998)). Eq. (2) can be rewritten as:

$$\ln\{A(f, t) \cdot t^\alpha\} = \ln\{S(f)\} - \frac{\pi \cdot f \cdot t}{2 Q_C}. \quad (3)$$

The Q_C value is determined at different frequency bands from the slope of the linear equation fitting between the logarithm coda amplitudes $\ln\{A(f, t) \cdot t^\alpha\}$ and time t . According to (Rautian and Khalturin, 1978), the above relations are valid for lapse times greater than twice the S-wave travel time (Fig. 4).

It has been observed that the coda spectrum of small earthquakes for near source records is independent of the earthquake size and that the path length between the station and the epicenter (and therefore maximum depth reached by the rays) depends on the lapse time from the origin time of the earthquake (Aki and Chouet, 1975; Sato, 1977). This suggests that the coda part of the seismogram results mostly from an average scattering effect of the medium in the region between the source and the station. By using the single backscattering model, we can approximately evaluate the depth of the coda wave formation (Pulli, 1984). Indeed, according to Pulli (1984), the obtained Q_C value characterizes some volume of the lithosphere, presumably ellipsoidal, where the source and the seismic station are located at the foci of the ellipsoid. The dimensions of this area are determined from simple geometrical considerations:

$$a = \frac{V_\beta \cdot t_a}{2}, b = \sqrt{a^2 - \frac{r^2}{4}}, c = b + h, \quad (4)$$

where a and b are the largest and the smallest axes of surface projection of the ellipsoid, c is the lower border of the ellipsoid, V_β is the S-wave velocity and it is equal to 3.55 km/s (Golenetsky and Novomeiskaya, 1975), r is the distance from the source to the receiver, h is the earthquake depth, t_a is the average length of the time window. The t_a is determined as $t_a = (t_{start} + \frac{W}{2})$, where t_{start} is the origin time for the coda processing, and W is the length of the lapse time window. In other words, the sizes of the area studied are dependent on the lapse time window and on the distance 'source–receiver'. Thus, by changing the lapse time window W or epicentral distances, we check and follow the change of $Q_C(f)$ values with depth. In our study, the attenuation parameters are determined using events occurring within a wide area (Fig. 3) with different seismic paths and epicentral distances. In this case, the Pulli's method only provides an average evaluation of the depth of coda wave formation.

The amplitude of the body seismic wave A at distance r for a bandpass-filtered seismogram at the central frequency f is related to the attenuation parameter Q_S by the following relation (Bath, 1974):

$$A(r) = A_0 \cdot r^{-\alpha} \cdot e^{-\frac{\pi f r}{2 Q_S V_\beta}}, \quad (5)$$

A_0 is the seismic wave amplitude in the earthquake source, α is the geometrical spreading parameter, as mentioned above $\alpha = 1$ for body waves (Sato and Fehler, 1998). Eq. (5) may be rewritten in analogy to Eq. (3):

$$\ln\{A(r) \cdot r^\alpha\} = \ln\{A_0\} - \frac{\pi \cdot f \cdot r}{2 Q_S(f) \cdot V_\beta}. \quad (6)$$

The Q_S value is determined at different frequency bands from the slope of the linear equation fitting between the logarithm S-wave amplitudes $\ln\{A(r) \cdot r^\alpha\}$ and distance r .

For Q_C -values estimation, 274 local events with magnitude $M_L = 3.1$ –5.4 that occurred within the Baikal rift were selected (Fig. 3). The hypocentral distances of the events mainly range from 15 to 200 km, in some cases reaching 700 km (Table 1). Most seismic 'source–receiver' paths crosscut the rift structures. To evaluate the quality factor the seismic records obtained on all three components were used: Q_C -values were estimated partly for each component and then they were averaged. The time of the onset of signal processing was taken at twice the S-wave travel time and lapse time windows were taken from 10 to 100 s with a step of 5 s. For Q_C -values estimation we used the records of direct S-waves of sixteen strong local earthquakes (body-wave magnitudes $m_b = 5.0$ –6.0) that occurred within the rift system for the period 2003–2006; the epicentral distances Δ change within 20–169 km (Table 2). The seismic traces were processed by Butterworth filter at six frequency ranges: 0.3 ± 0.2 , 0.75 ± 0.25 , 1.5 ± 0.5 , 3 ± 1 , 6 ± 2 and 12 ± 4 Hz (Fig. 4). The use of a relatively narrow frequency range

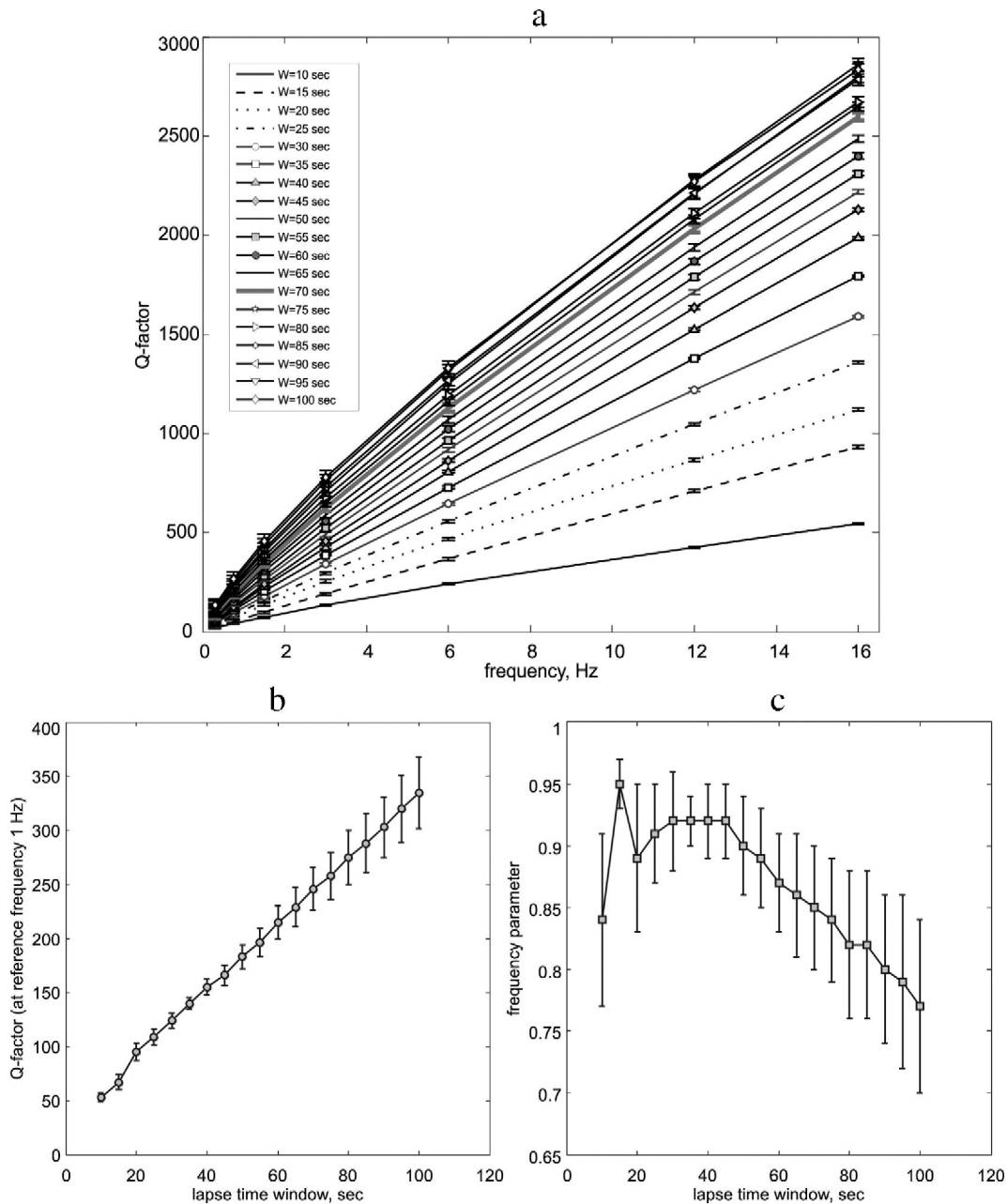


Fig. 7. (a) Plot of the mean Q_c values of each lapse time window versus frequency. (b) Quality factor Q_0 at the frequency of 1 Hz versus lapse time window W . (c) Frequency parameter n versus lapse time window W . Root mean square deviations are given for each value.

is due to the fact that we tried to carry out measurements within the flat part of the frequency response, so that there was no distortion of the seismic signal. In the calculation of Q_s -values, the maximum displacement amplitude (A_s) and the corresponding frequency were measured on the filtered traces and the displacement amplitude for different earthquakes were recomputed for the same magnitude. Finally, Q_s -value is determined based on the slope of the least-square straight-line fit between the maximum amplitude A_s versus the epicentral distance Δ for each frequency range (Fig. 5).

4. Results

Our Q_c -factor determination is based on the processing of 2579 waveforms (Table 1). Q_c -values were estimated for 19 lapse time windows ranging from 10 to 100 s with a step of 5 s and for 6 frequency ranges: 0.3 ± 0.2 , 0.75 ± 0.25 , 1.5 ± 0.5 , 3 ± 1 , 6 ± 2 and 12 ± 4 Hz

(Table 3). In total, we have determined 112 Q_c values. There are no Q_c -factor values for the minimum central frequency 0.3 Hz for the lapse time windows 10 and 15 s because the lengths of the windows are too short. Standard deviations change within a wide range – from 18 to 113% (Table 3), however a large number of measurements (94) are characterized by relatively low standard deviations (18–45%). Twelve Q_c -measurements have standard deviation values within the range 46–60% and only 6 have standard deviations exceeding 60% (Table 3). The maximum values of standard deviations are observed for low frequencies and for short lapse time windows (Table 3): this is related to the lack of data (peak amplitudes) preventing a reliable determination of the approximation straight line position for small windows and low frequencies. In further calculations, the Q_c -values with a standard deviation exceeding 60% were not considered.

The average Q_c value increases with the frequency and lapse time window, from 46 ± 52 (at 0.75 Hz) to 502 ± 109 (at 12 Hz) for $W =$

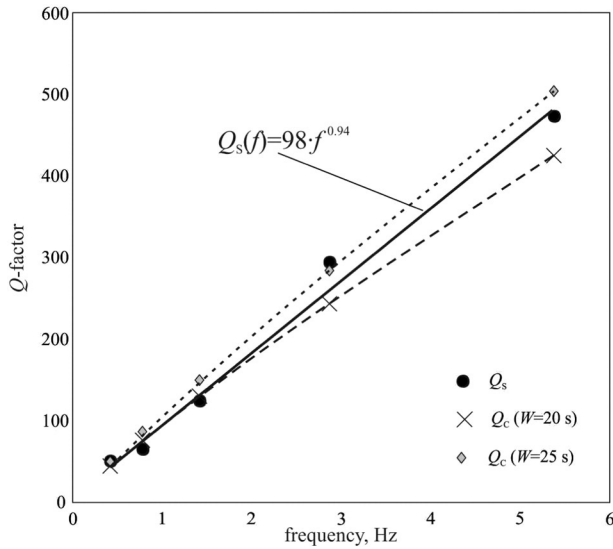


Fig. 8. Comparison of $Q_c(f)$ and $Q_s(f)$ ratios.

10 s, and from 114 ± 49 (at 0.3 Hz) to 1865 ± 679 (at 12 Hz) for $W = 100$ s (Table 3, Fig. 6). For all the lapse time windows, empirical relations $Q_c(f)$ are obtained according to the ordinary power law (1) (Table 4, Fig. 7a). Quality factor Q_0 increases with lapse time window (Table 4, Fig. 7b). At the same time, more complex behavior is observed for n -values: for lapse time windows of 10–25 s, 25–45 s and >45 s, n -values are changing sharply, are stable and are decreasing, respectively. As mentioned above, the frequency parameter characterizes the heterogeneity of the medium and the level of tectonic activity (Aki and Chouet, 1975; Sato and Fehler, 1998; Mak et al., 2004; Sato et al., 2012). Furthermore, its variations are theoretically connected to the medium heterogeneity at different depths (Pulli, 1984).

The Q_0^{-1} values were determined for six frequency ranges: 0.1–0.5; 0.5–1.0; 1.0–2.0; 2.0–4.0; 4.0–8.0 and 8.0–16.0 Hz (Fig. 8). The comparison of $Q(f)$ ratios for the direct waves and coda is presented in Fig. 8.

The Q_s -values characterize only Earth's crust in contrast to Q_c since direct body S -waves propagate in crust only while coda waves may propagate in the lithosphere below Moho. Therefore, Q_s values may be compared with Q_c values obtained for the shortest lapse time windows for which the attenuation effects below the Moho may be neglected. At low frequencies (0.1–8.0 Hz), $Q(f)$ ratios for S and coda-waves fit well: $Q_s(f) = (98 \pm 15) \cdot f^{(0.93 \pm 0.05)}$ and $Q_c(f) = (95 \pm 8) \cdot f^{(0.89 \pm 0.06)}$ for the lapse time window $W = 20$ s, and $Q_c(f) = (109 \pm 7) \cdot f^{(0.91 \pm 0.04)}$ for $W = 25$ s. The consistency of the Q -value of direct shear waves and coda is an additional evidence that the coda waves are scattered and reflected from the heterogeneities of the lithosphere (Aki and Chouet, 1975).

Lithosphere structure of the Baikal rift system is significantly inhomogeneous. Various segments of the rift system have developed differently, depending on their geometry and orientation relative to the main stress directions, on the age and structural inheritance of the basement or on the more or less anomalous state of the mantle. The current stage of development of the Baikal rift system depicts also some relative inhomogeneity, as shown by differences in the seismic activity or in the velocity field of its segments since Late Cenozoic times (Petit et al., 1996; San'kov et al., 1997, 2000, 2009; Calais et al., 2003; Radziminovich et al., 2013). These factors may all contribute to lateral variations in seismic wave attenuation.

In order to estimate these lateral variations, we compute an attenuation quality factor (Q_c) within different tectonic units of the Baikal rift system: rift basins, range uplifts, spurs, and the Siberian Platform. The regionalization is based on the identification of the main morphotectonic units and on the presence of enough initial data (i.e., earthquakes). As a result, 22 blocks were selected (Table 5, Fig. 9). The main earthquake selection criterion was the lateral co-location of seismic stations and earthquakes epicenters: for each morphotectonic unit, earthquakes occurring within it were selected. The records obtained by the seismic station located within this structure or on its boundaries (in case of basins filled by water) were used for calculations.

For each block, we have computed values of the frequency parameter and quality factor at a frequency of 1 Hz (Table 5). This frequency was selected because for this frequency, heterogeneity of attenuation field is most evident (Aptikaeva and Kopnichev, 1991). Along the rift

Table 5
Quality-factor and frequency parameter for different tectonic structures of the Baikal rift system.

Block	Tectonic structure	Q_0	σ_{Q_0}	n	σ_n	N	$\Sigma M_0 \cdot 10^{16}$, N·m	$M_{0max} \cdot 10^{16}$, N·m	Fault density	heat flow, mW/m ²	
										Max	Mean
1	2	3	4	5	6	7	8	9	10	11	12
1	Eastern Sayan uplift	94	6	0.96	0.04	154	30.909	3.436	110	143	95.25
2	Khamar-Daban uplift	121	16	0.84	0.08	84	36.422	8.035	70	69	57.00
3	Tunka basin	96	7	0.91	0.04	140	28.637	8.035	70	103	80.00
4	Main Sayan fault	84	7	1.1	0.07	68	7.878	1.107	90	103	80.00
5	Siberian platform	134	26	0.48	0.12	13	12.403	1.469	50	64	39.54
6	South Baikal basin	95	11	0.89	0.08	189	113.548	14.158	130	165	67.63
7	Central Baikal basin	89	5	0.99	0.04	195	85.644	2.588	170	264	71.32
8	North Baikal basin	109	12	0.88	0.09	84	28.729	4.560	70	474	81.23
9	Upper Angara basin	89	2	0.97	0.02	118	126.852	10.666	70	330	89.82
10	Kitchera–Upper Angara spur	96	14	0.94	0.09	89	93.739	10.666	70	79	55.33
11	Barguzin uplift	93	9	0.91	0.07	270	154.095	3.436	110	330	128.33
12	Barguzin basin	97	5	0.95	0.03	98	35.320	6.053	170	152	90.00
13	Ikat uplift	100	5	0.92	0.04	84	47.661	2.588	110	79	79.00
14	Kitchera basin	99	9	0.87	0.05	65	25.742	3.436	110	56	32.00
15	North-Muya uplift	102	9	0.95	0.07	15	13.905	2.588	90	64	41.50
16	Upper Angara - Muya spur	72	4	0.98	0.04	28	27.734	1.950	70	147	85.67
17	North-eastern part of Upper Muya basin	72	4	1.22	0.05	96	81.693	18.793	70	147	77.00
18	Tsipa-Baunt basin	76	9	1.03	0.07	60	13.051	1.950	90	147	49.00
19	Muya basin	94	13	0.89	0.08	40	11.827	1.469	70	58	41.75
20	Chara basin	99	5	0.92	0.03	81	110.907	18.793	70	48	28.75
21	North-eastern part of Udokan uplift	97	15	0.79	0.2	24	47.055	14.158	70	78	50.80
22	Udokan uplift	109	10	0.85	0.06	91	21.335	3.436	110	78	43.67

Comment: 1, 2 – number and name of tectonic structure (see Fig. 11), 3, 4 – quality factor at the reference frequency $f_0 = 1$ Hz and its standard deviation, 5, 6 – frequency parameter and its standard deviation, 7 – number of measurements, 8, 9 – summary and maximum seismic moment realized within this structure since 1960, 10 – maximum fault density, and 11, 12 – maximum and mean values of the heat flow, registered within this structure and the nearest environment.

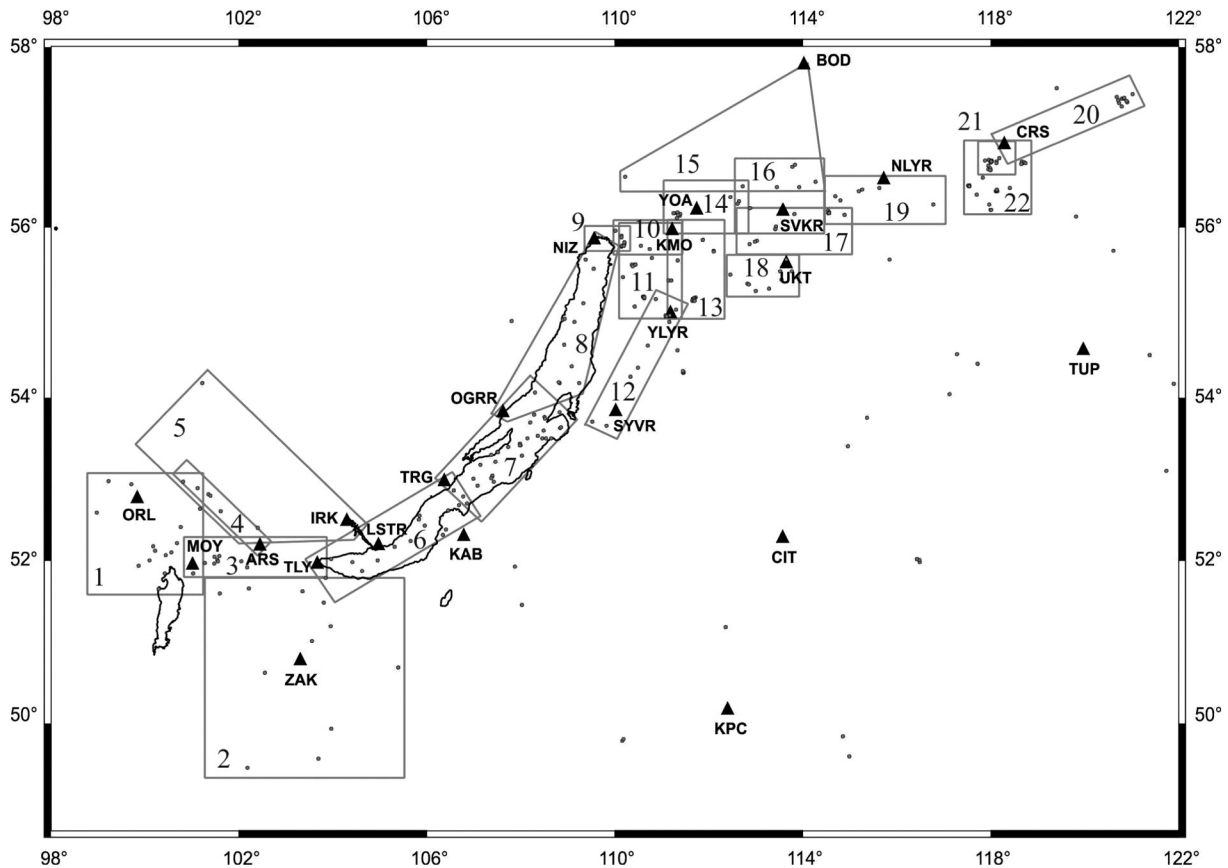


Fig. 9. Areas selected for estimation of attenuation parameter.

system, Q_0 varies within 72–109 and the n -value changes from 0.87 to 1.22 (Table 5). Low value of Q_c -factor (84) and high value of n (1.1) are observed for the Main Sayan fault. In general, minimum values of Q_c -factor are observed for rift basins, and maximum values for the spurs and the uplifts (Table 5).

The attenuation parameters obtained in the present study satisfactorily agree with those obtained earlier for more specific parts of the Baikal rift system. Indeed, values of the attenuation coefficient ($\delta = 0.0060 \pm 0.0010$) and the Q_c -factor ($Q_0 = 150, f = 1$ Hz) for the Siberian Platform (see Table 5 and Dobrynina et al., 2011 and references therein) agree with those obtained in the present study ($\delta = 0.0066 \pm 0.0013$ km⁻¹ and $Q_0 = 134 \pm 26$). This is also the case for the upper crust in the NE Baikal rift ($Q_c = 140$ at $f = 1.7$ Hz, against our value of $Q_c = 145 \pm 51$ at $f = 1$ –2 Hz, see Table 3). Zones of faulting in the upper crust are known to represent areas with specific physical and rheological patterns differing from those of more “intact”, cold, old or anhydrous crustal blocks (Sherman, 1978; Fagereng, 2013). These changes are mainly reflected in the strength, density, metamorphic and anisotropic properties. In the present work, we attempt to estimate the attenuation parameters of coda waves close to large active faults. For this purpose, we selected a set of large faults south of the Siberian Platform: the Obruchev, Primorsky, Tunka and Main Sayan faults (Fig. 10), since the distribution of the seismic stations and earthquake epicenters is the best possible in this area. Quality-factor values for the paths crossing the fault zone were calculated. The attenuation coefficients obtained were compared with those of surrounding tectonic blocks. Attenuation coefficient ($\delta = 0.011$ km⁻¹) was determined for the Main Sayan fault only as the seismic station (TLY), and earthquake epicenters were located within its area so that seismic rays cross the fault body and not areas of the Siberian Platform and the Eastern Sayan (Fig. 10f). For earthquakes occurring in the South Baikal Lake, Q -factor and attenuation coefficient δ are estimated for the stations

situated near the shores of the basin – Talaya (TLY), Listvyanka (LSTR), Tyrgan (TRG) and Kabansk (KAB) (Fig. 10b). The maximum values of δ (0.012–0.013 km⁻¹) were obtained for seismic stations TLY (situated within the Main Sayan fault zone), LSTR (near the Obruchev fault) and TRG (near the Primorsky fault). For seismic station KAB, δ is lower (0.008 km⁻¹), although average distances ‘source–receiver’ for all the stations mentioned above are equal. For seismic path ‘Baikal–Primorsky fault–Siberian Platform–Irkutsk (IRK)’, δ is higher than for the Siberian Platform – 0.0093 and 0.0066 km⁻¹ respectively (equal epicentral distances, Fig. 10c). An increase in attenuation coefficient (~60%) for the seismic path ‘Main Sayan fault–Tunka fault–Zakamensk (ZAK)’ in comparison with the path ‘South Baikal–ZAK’ is observed (Fig. 10d). The former path crosses the Tunka fault, whereas the second one propagates along the intrabasin faults of the South Baikal basin. Also, an increase in δ value (~25%) is observed for the path ‘Tunka basin–Tunka fault–Main Sayan fault–Siberian Platform–IRK’ in comparison to the path ‘Main Sayan fault–Siberian Platform–IRK’ (Fig. 10e). Thus we observe that attenuation coefficient δ abruptly increases when crossing zones of large active faults by an average value of 20–60% compared to the “intact” block interiors. Furthermore, the attenuation across an active fault zone is greater than along strike. This is indeed a clear indication that the rock medium is anisotropic with respect to the seismic wave attenuation.

5. Discussion

5.1. Comparison with other regions with various tectonic activities

The frequency dependence of attenuation (parameter n) obtained in this study indicates that the upper lithosphere of the Baikal rift system is highly heterogeneous (Table 4). Values Q_0 and n obtained vary from 53 ± 4 to 335 ± 33 and from 0.84 ± 0.07 to 0.77 ± 0.07 respectively,

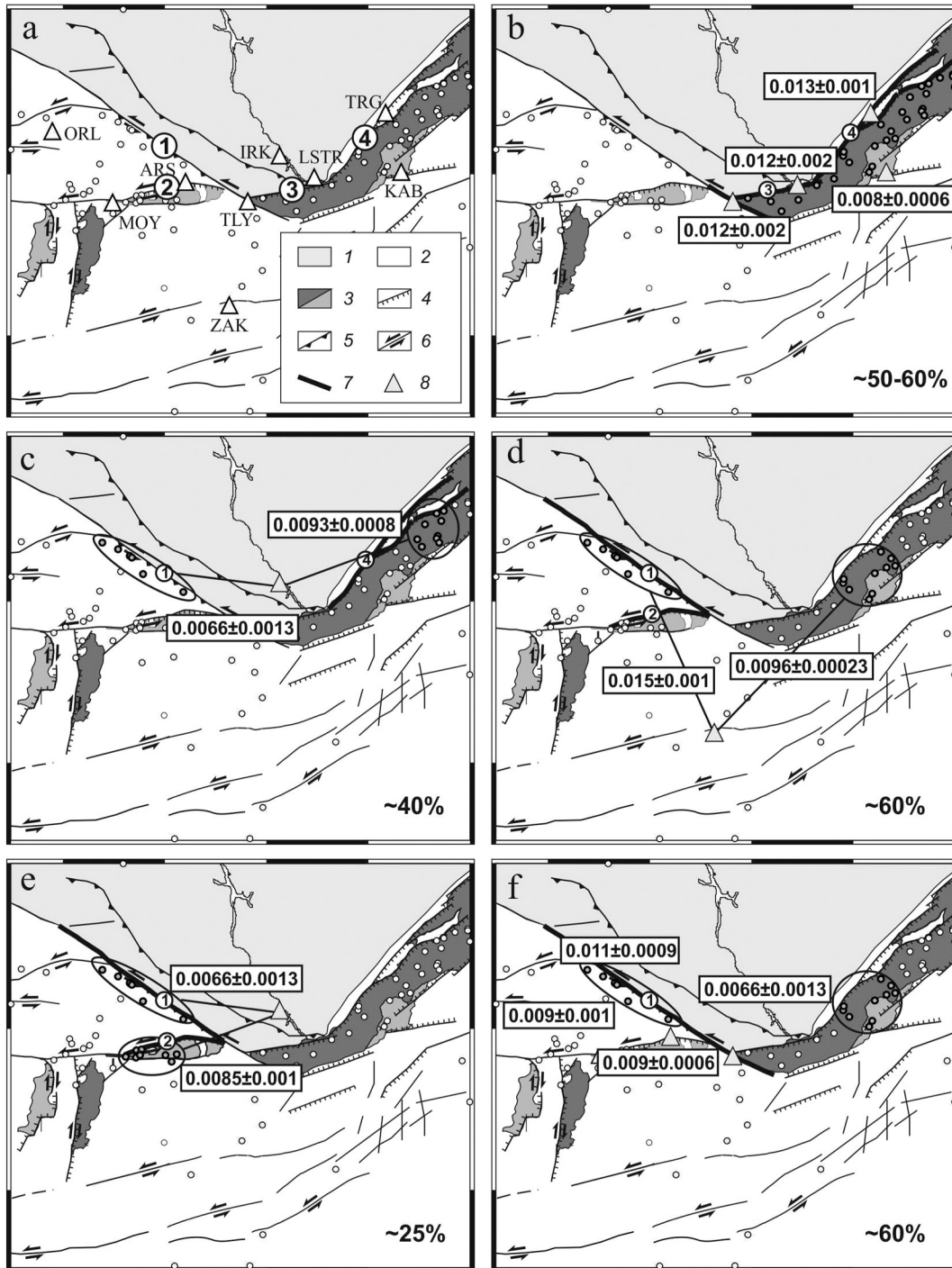


Fig. 10. Distribution of the attenuation coefficient δ (km⁻¹) in zones of main active faults and their surroundings. (a) Location of stations (letter codes) and main faults (numbers in circles): 1. Main Sayan, 2. Tunka, 3. Obruchev, 4. Primorsky. Inset: 1. Siberian platform; 2. Sayan-Baikal folded area; 3. Cenozoic rift basins; 4–6. Faults (normal, thrust, strike-slip, respectively); 7. Studied fault; 8. Seismic station and ray path “station-selected earthquakes”. (b) to (f): attenuation coefficient δ computed: (b) Primorsky and Obruchev faults, (c,d) Primorsky and Main Sayan faults, (e) Main Sayan and Tunka faults, and (f) Tunka, Main Sayan and Primorsky faults. Earthquakes are shown by circles, seismic stations by triangles. Increase of attenuation coefficient for the studied fault relative to neighboring blocks is shown by percent (right bottom angle).

depending on lapse time window (Table 4). Such values are usual for regions with high tectonic activity (Singh and Herrmann, 1983, Mak et al., 2004). They fall in the same range than the ones determined for the Basin and Range Province and the Kenya rift, i.e. Q_0 from 60 ± 8 to 222 ± 17 and from 74 ± 3 to 278 ± 48 , n from 0.57 ± 0.04 to 0.84 ± 0.05 ($W = 10-95$ s) and from 1.12 ± 0.02 to 0.93 ± 0.11 ($W = 20-80$ s), respectively (Dobrynina, 2013; Dobrynina et al., 2012).

The empirical $Q_C(f)$ relations obtained in the present study are compared with those for regions with different tectonic conditions and level

of seismic activity, i.e. (1) areas with stable and moderate tectonics (Fig. 11a) and (2) areas with high tectonic activity (Fig. 11b). Regions with moderate and stable tectonic activity (e.g. North American Platform, Canadian Shield, North Iberia) depicts $Q_C(f)$ values that clearly differ from those with high tectonic activity (e.g. India, Himalaya, Japan, California). As expected, the $Q_C(f)$ obtained for the Baikal rift is similar to the ones found in areas with high tectonic activity. At the same time, the frequency parameter obtained for the Siberian Platform ($n = 0.48$) matches n values found for stable or weakly deforming

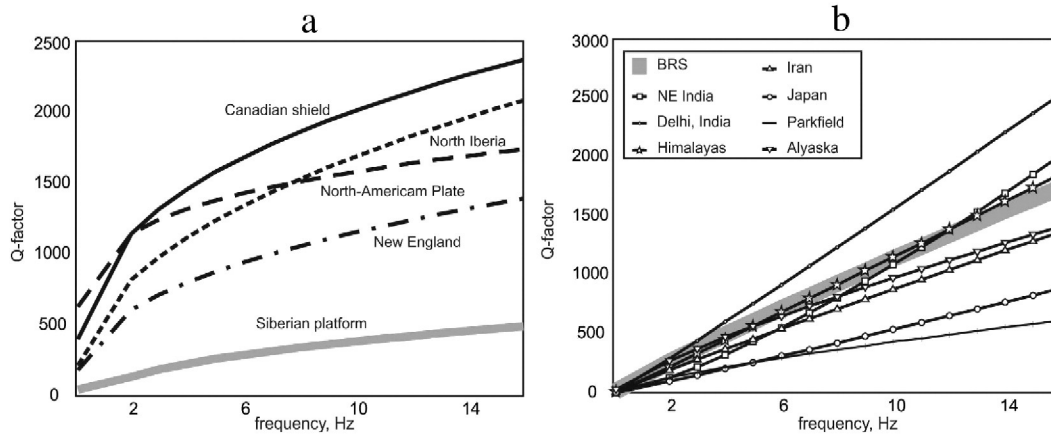


Fig. 11. Comparison of relations $Q_c(f)$ of the Baikal rift and surroundings with those estimated for other parts of the world. (a) Stable zones (or with moderate tectonics): south of Central Alaska ($Q_c(f) = 158f^{0.79}$) (Dutta et al., 2004), New England ($Q_c(f) = 460f^{0.4}$) (Pulli, 1984), North Iberia ($Q_c(f) = 600f^{0.45}$) (Pujades et al., 1991), Canadian Shield ($Q_c(f) = 900f^{0.35}$) (Hasegawa, 1985), North American Platform (Central USA) ($Q_c(f) = 1000f^{0.2}$) (Singh and Herrmann, 1983), Siberian Platform ($Q_c(f) = 134f^{0.48}$) (the present work); (b) zones with active tectonics: North Eastern India ($Q_c(f) = 52f^{1.32}$) (Hazarika et al., 2009), Delhi, India ($Q_c(f) = 142f^{1.04}$) (Mohanty et al., 2009), Himalayas ($Q_c(f) = 110f^{1.02}$) (Gupta and Kumar, 2002), Central Iran ($Q_c(f) = 101f^{0.94}$) (Ma'hood and Hamzehloo, 2009), Japan ($Q_c(f) = 47f^{1.06}$) (Matsumoto and Hasegawa, 1989), Parkfield, California ($Q_c(f) = 79f^{0.74}$) (Hellweg et al., 1995), the Baikal rift system ($Q_c(f) = 124f^{0.92}$) (present work) for the same lapse time windows $W = 30$ s for all regions according to Gusev (1995).

areas (Fig. 11a) such as North Iberia ($n = 0.45$) (Pujades et al., 1991), the Canadian Shield ($n = 0.35$) (Hasegawa, 1985) and New England ($n = 0.40$) (Pulli, 1984).

5.2. Vertical variations of attenuation

The tendency to the decrease in n -values and increase in Q_c -values with increasing lapse time may reflect the heterogeneity of the medium in the upper lithosphere or may be also an effect of multiple scattering for longer lapse times (Gao et al., 1983). Here, we have analyzed the data for lapse time windows up to 100 s, therefore this effect of multiple scattering is likely moderate (Sato et al., 2012). Such behavior of attenuation parameters with lapse time has also been interpreted as an effect of depth (Roecker et al., 1982; Pulli, 1984; Kvamme and Havskov, 1989; Gusev, 1995). In our case study, attenuation of direct S-waves and coda waves (at small lapse time windows) is similar, which suggests that the coda is dominantly built with reflected shear waves arising from inhomogeneities in the medium. The approach by Pulli (1984) using relations (4) is therefore considered as suitable to evaluate the depth of penetration of coda waves. The average epicentral distance for the selected events is about 220 km and the average value t_{start} is 68 s. Since there are no reliable data on the earthquake depths for the selected events, we have used the average depth $h = 15$ km (Radziminovich, 2010 and references therein). The lowest depth values of the ellipsoid (or depth of coda formation) vary from 83 down to 193 km (Table 6).

Table 6
The ellipsoid axes (a, b, c) with the lapse time window.

W , sec	a , km	b , km	c , km	W , sec	a , km	b , km	c , km
1	2	3	4	1	2	3	4
10	130	68	83	60	174	135	150
15	134	77	92	65	178	140	155
20	138	84	99	70	183	146	161
25	143	91	106	75	187	152	167
30	147	98	113	80	192	157	172
35	152	105	120	85	196	162	177
40	156	111	126	90	201	168	183
45	161	117	132	95	205	173	188
50	165	123	138	100	209	178	193
55	170	129	144				

Comment: 1 – lapse time window (in sec), 2 – the largest axis, 3 – the smallest axis, and 4 – the depth of ellipsoid's lower border.

Our suggestion of the causal link between lapse time window and depth is based on results by Pulli (1984) that has shown that the increase of lapse time windows is coeval to the depth increase. The smallest lapse time window used by us corresponds to volume exceeding the thickness of the crust. We believe that if the coda generation occurred only in the crust, then the lateral increase of number of scatterers should be linked to an increase of attenuation with increasing lapse time window, while we observe the opposite. This effect may be reached only by an increasing coda-wave penetration depth since the lithosphere becomes more homogeneous with depth (Pulli, 1984; Kopnischev and Sokolova, 2004, 2012; Irandoust et al., 2016).

The attenuation coefficient δ and the frequency parameter n are observed to behave differently with depth (Table 4, Fig. 12). The δ -value decreases with depth according to the power law: $\delta = 143.73 \cdot c^{-2.083}$, the largest changes in the δ -value coinciding with the upper part of the lithosphere (Fig. 12c). The power dependence between δ and c is the evidence that the decrease in the attenuation with depth in the upper part of the lithosphere is faster than in its lower part.

Changes of the frequency parameter with depth are more complex (Fig. 12b). At depths of 83–113 km, there is a gradual increase in the n -values from 0.84 to 0.91, while at the depth of 77 km there is a jump in n to 0.95 (the largest value of n). In the depth interval from 113 to 132 km, n -value remains constant ($n = 0.92$). Then, n decreases down to 0.77 from 132 km to 193 km depth. The maximum gradient coincides with the upper part of the lithosphere, as for the attenuation coefficient (Fig. 12c, d). Heterogeneity of the medium tends to decrease with depth. Along with, an increase in parameter n at depths of 83–113 km may indicate the existence of numerous horizontal discontinuities associated with plate motion, coinciding with a sharp decrease in the electrical conductivity under the Baikal rift system found at 80–130 km depth (Pospeev, 2012). Besides, the constant value of the frequency parameter in the layer 113–130 km is likely to reflect asthenospheric flow with the same vertical velocity gradient.

Two-dimensional teleseismic travel time tomography along strike of the rift system has evidenced a high-speed limit at a depth of about 100 km (Mordvinova, 2009). It is well expressed in the northern rift system and can be traced discontinuously in the central and southern rift (Mordvinova, 2009; Anan'in et al., 2009). Values of δ - and n gradients depict sharp changes at depth of about 90–100 km (Fig. 12c, d), i.e. within this velocity discontinuity. Similar behavior of δ and n with depth was noted in the south Kenya rift and the Basin and Range Province (Dobrynina, 2013; Dobrynina et al., 2012). Thus, the change in attenuation parameters with depth is clearly related to the velocity

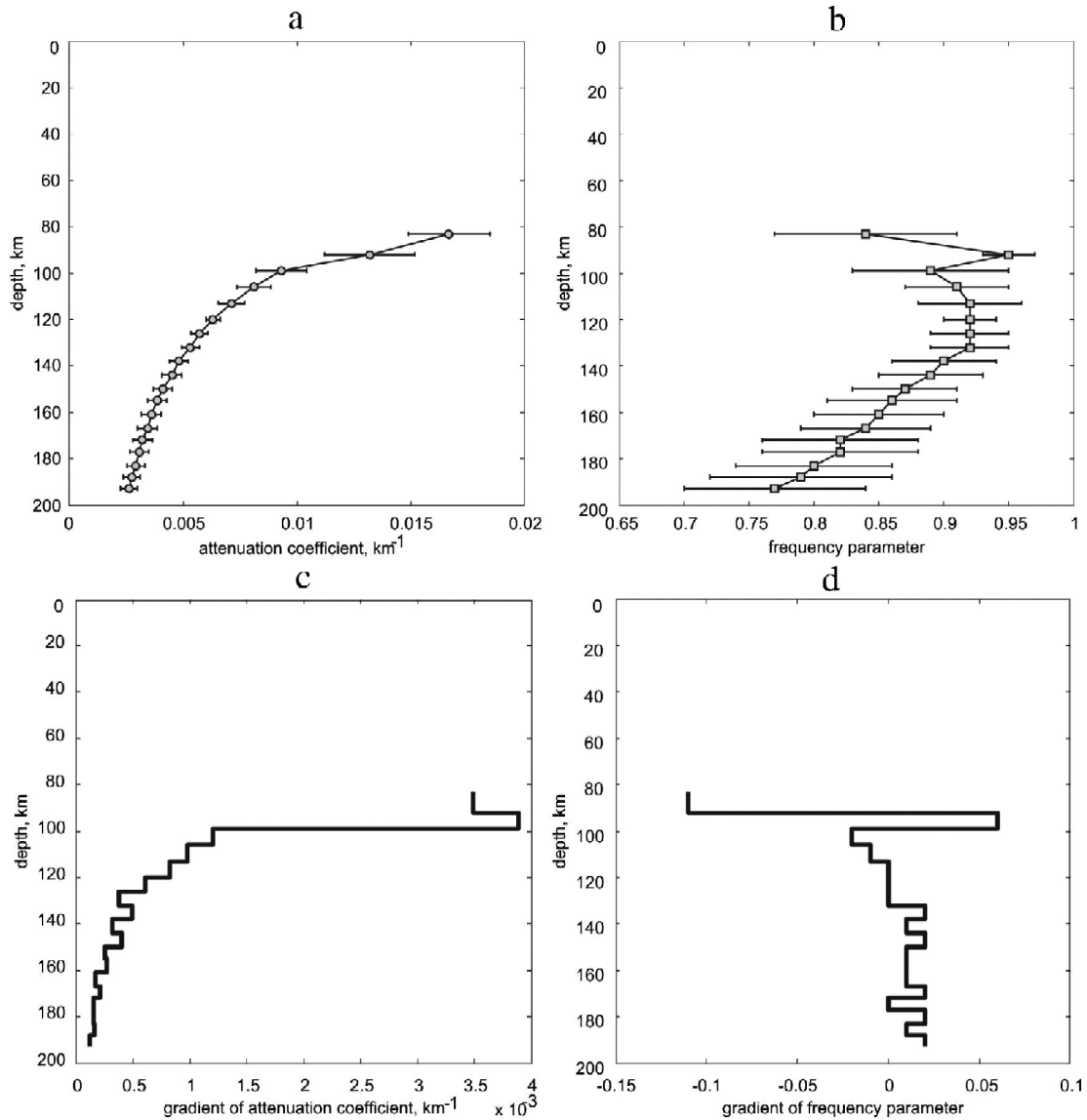


Fig. 12. Vertical variations of the attenuation parameters: attenuation coefficient δ (a) and frequency parameter (b) versus depth of the lower boundary of the ellipsoid. Error on each value is shown. Bottom: gradients of the attenuation coefficient (c) and frequency parameter (d) versus depth.

change at the base of the lithosphere: sharp changes of δ and n values coincide with the lithosphere's discontinuities.

To summarize, low Q_c and high n values appear to reflect the faulted structure of the lithosphere but also the main discontinuities of the plate. The increase in Q_c values and decrease in attenuation coefficient δ and frequency parameter n with depth show that heterogeneity of the lithosphere decreases with depth (Pulli, 1984), probably because high pressure in the lower part of the crust results into closing cracks and plastic deformation (Nikolaevsky, 1984).

5.3. Lateral variations of attenuation

Previous results on lateral variations of coda wave attenuation for the south-western part of the Baikal rift system (Dobrynina et al., 2011) have highlighted the dependence of seismic wave attenuation on the seismic activity and in lesser degree on the age of the crust. The parameters Q_c and n show marked spatial and temporal variations, suggesting effects of geodynamic processes in the lithosphere such as precursors to strong earthquakes, fluid migration etc. (e.g. Aptikaeva, 1991; Kopnichev and Sokolova, 2012). In order to better highlight these

relationships, we attempt here to correlate the attenuation parameters obtained for different areas within the Baikal rift system (Table 5) with maps of cumulative seismic moment, surface fault density and heat flow.

Seismic moment, together with magnitude, is a major indicator of the energy of a seismic event, but has a physical dimension, in contrast to the magnitude. The seismic moments of 150 earthquakes (with M from 3 to 5) of the Baikal rift were obtained using a spectral analysis method and a correlation between seismic moment and local magnitude (Dobrynina et al., 2014). Based on the correlation ratio, the seismic moments were calculated for $M \geq 4$ earthquakes for the period 1960–2013, providing a 50×50 km grid map of cumulative seismic moment (Fig. 13). We have also used the map of the surface fault density in the Baikal rift (Sherman, 1992) which combines active and non-active faults (Fig. 14). A trapezoid with sizes of 65×70 km was taken per square unit. The number of faults in the trapezoid was taken to be the surface fault density. Finally, we have created a heat flow map based on the data published in Golubev (2000, 2007); Lysak (2002) and Duchkov (1985). Although points of heat flow measurements are distributed very unevenly (Fig. 15), the map clearly shows places of high

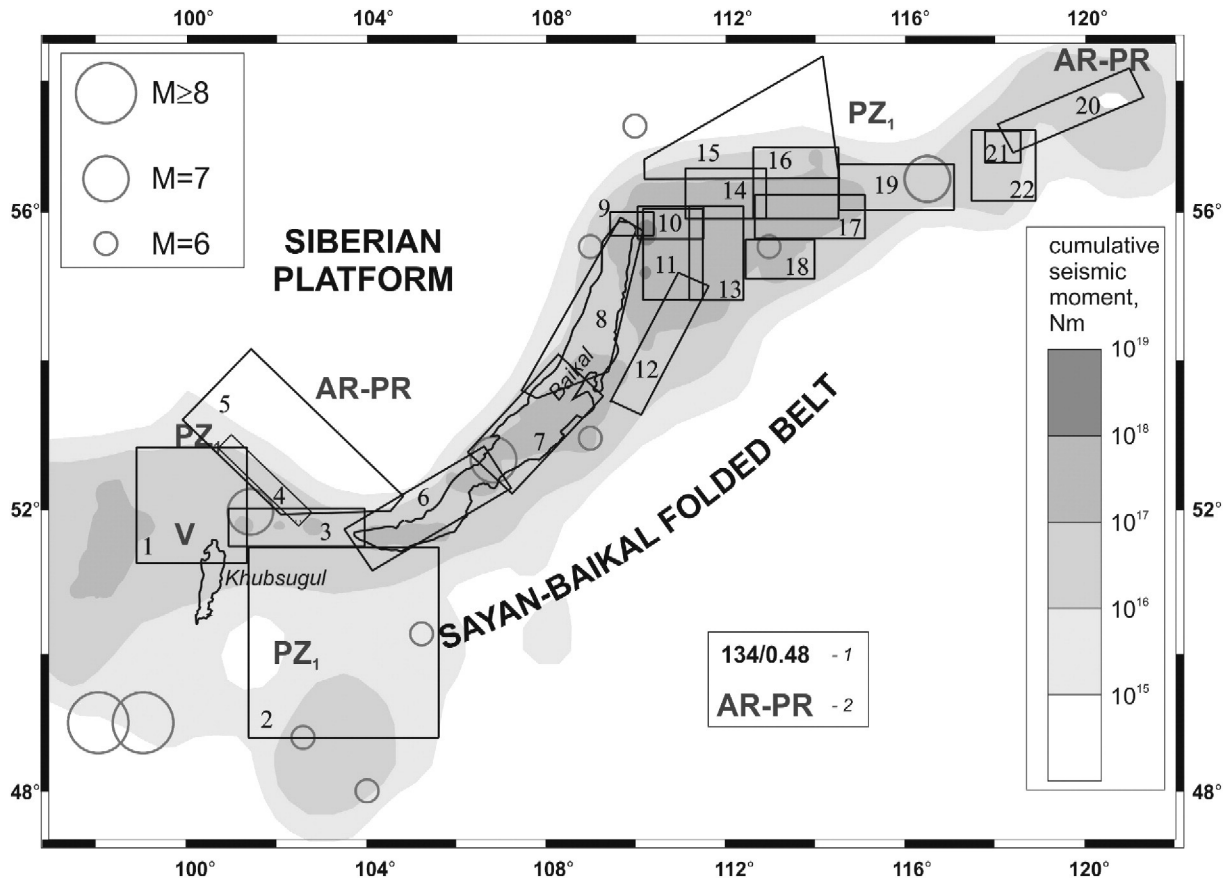


Fig. 13. Map of cumulative seismic moment (1960–2013) and spatial distribution of Q_0 (Q -factor at frequency 1 Hz) and n frequency parameter: 1. Q_0/n ; 2. Crustal age of tectonic blocks (AR-PR – Archean-Proterozoic, PZ1 – lower Paleozoic, V – Vendian). Strong earthquakes ($M \geq 6.0$) are shown by circles from historical (1905–1950) and instrumental (since 1950) data.

heat flow (e.g. edge of the Siberian Platform, Khubsugul basin and Barguzin-Muya regions). A comparison of maps of cumulative seismic moment, surface fault density and heat flow reveals a general good superimposition of anomalies: areas with high seismic activity (Fig. 13) are characterized by both a high density of faults (Fig. 14) and a high heat flow (Fig. 15). As a whole, the minimum values of the Q_c -factor coincide with the rift basins and the maximum values with the spurs and the uplifts, and areas with high values of cumulative seismic moment, high surface fault density and relatively high heat flow depict low values of the Q_c -factor and high values of frequency parameter.

In order to compare attenuation at the scale of individual tectonic structures, we have computed the maximum values of seismic moment and fault density on the one hand, and average and maximum values of heat flow on the other hand within selected blocks (Table 5). The comparison of maps of cumulative seismic moment (Fig. 13), surface fault density (Fig. 14) and heat flow (Fig. 15) with lateral distribution of quality factor (at reference frequency 1 Hz) and frequency parameter clearly evidences a spatial correlation of anomalies at this scale, in line with previous conclusions (Dobrynina, 2011; Dobrynina et al., 2011). On the one hand, attenuation and frequency parameter strongly decrease within ancient stable areas: the maximum values of the Q_c -factor (134) and the minimum values of the frequency parameter n (0.48) are observed for the aseismic Archean–Proterozoic Siberian Platform characterized by low heat flow and low surface fault density (Table 5, Figs. 13–15), and Q is low in the Paleozoic Khamar–Daban block and the Pre-Cambrian Muya block. On the other hand, the Q -factor also decrease for both the Archean–Proterozoic and Lower Paleozoic blocks when the rift structures are imposed on it (e.g., Chara basin which developed within the Siberian Platform depict Q_c -values of 99 and n -values of 0.92). Furthermore, no significant effect of the thinning of

the lithosphere is observed: in the South Baikal basin where an asthenosphere upwelling is suggested (Gao et al., 1994; Mordvinova, 2009; Mordvinova and Artemyev, 2010), the values of Q -values and n -values are comparable to those for the neighboring basins with thicker lithosphere (Table 5, Figs. 13–15).

However, two areas depict different patterns of anomalies, the Muya region and the North Baikal basin. In the Muya region (including blocks 16–18: Upper Angara–Muya spur, NE part of the Upper Muya basin and Tsipa–Baunt basin), the Q_c is the lowest (72) and n is the highest (1.22), which agrees with the high seismic activity of this part of the rift system. However, the surface fault density is relatively low (~ 70), in contrast with high n -value. On the other hand, local heat flow anomaly (147 mW/m^2) may well explain high attenuation of seismic waves in this area (Aptikaeva, 1991; Kopnichev and Sokolova, 2012). The North Baikal basin is also a contrasted area, with a high heat flow (474 mW/m^2 , Fig. 15), a very low seismic activity (in the instrumental and historical time period), and a low fault density (Figs. 13, 14). It is characterized by high value of Q_c (109) and relatively low value of the frequency parameter ($n = 0.88$). From these two case studies, we suggest that high heat flow may be dominant upon other parameters and thus lead to an increase in attenuation, whereas our record of the seismic activity may be too short for some regions of the rift system such as the northern Lake Baikal (Déverchère et al., 1993; San'kov et al., 2000), leaving open the hypothesis of a seismic gap in the region.

It remains that a major trend is the increase of the frequency parameter and attenuation in areas with high seismic activity, surface fault density and heat flow (Fig. 16), suggesting that Q_c and n may be used as tectonic activity indicators. The deformation of the lithosphere under tension favors convective heat transfer, inducing a significant modification of the properties of the lithosphere, regardless of the age

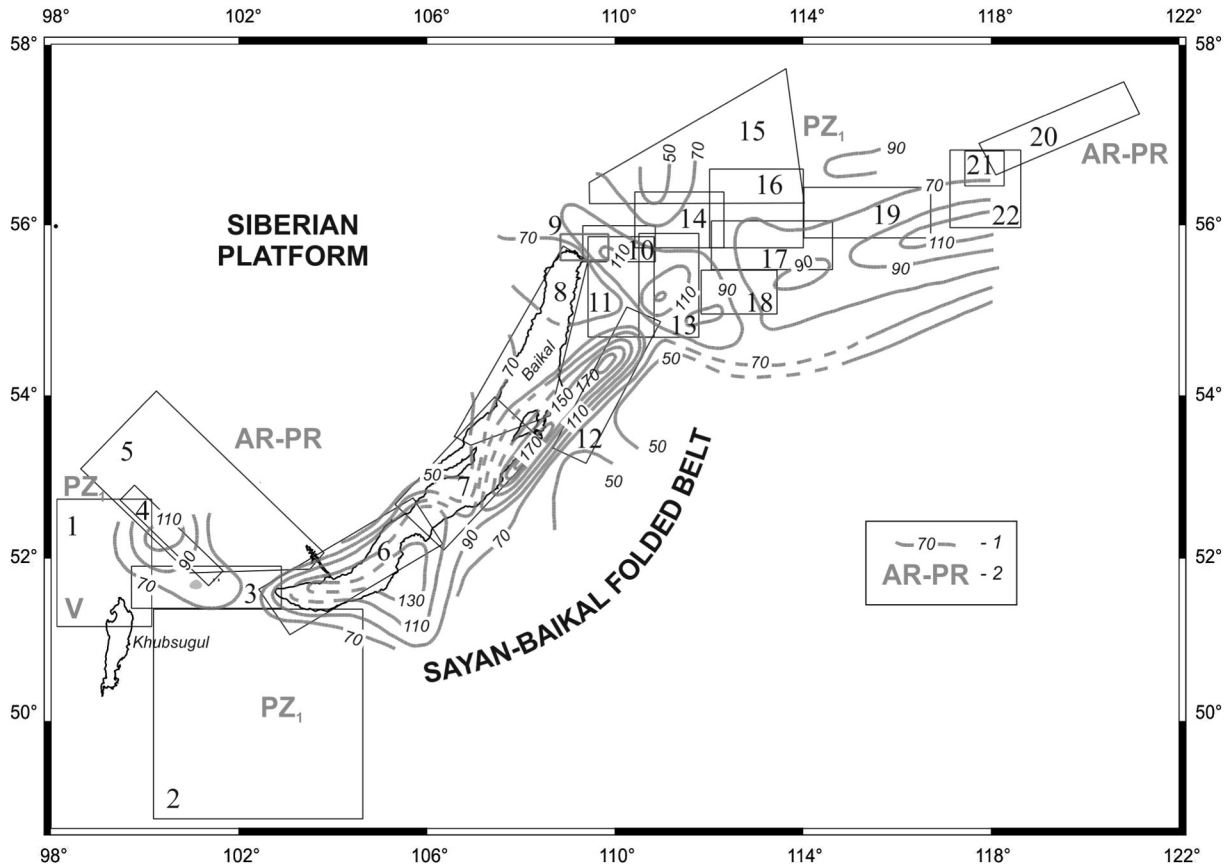


Fig. 14. Map of surface fault density (Sherman, 1992) and spatial distribution of Q_0 (Q -factor at frequency 1 Hz) and frequency parameter n : 1. Q_0/n ; 2. Isolines and values of fault frequency; 3. Crustal age of tectonic blocks (same as Fig. 13).

of the crust. Thus, we believe that the elastic properties of the lithosphere are substantially changed by the effects of the rifting processes, whereas in old blocks not affected by rifting, attenuation and the frequency parameters remain lower than in rift basins and mountain uplifts (Fig. 16g, h).

5.4. Attenuation in shear zones

High strain rates of the lithosphere generally lead to the formation of a dense network of faults. Clearly, seismic attenuation increases with fault density (Fig. 16), revealing an increase in the heterogeneity of the medium with brittle and brittle-plastic deformations. Similar changes with the degree of seismic activity (Fig. 16) have been interpreted since long to reveal the influence of the level of tectonic and seismic activity on the attenuation of seismic waves (e.g., Aki and Chouet, 1975; Aki, 1982; Sato and Fehler, 1998; Mak et al., 2004). Our study shows that within the same tectonic structure (the Baikal rift system) and also at the scale of individual morphotectonic structures or fault systems (Figs. 9–10 and 13–15, Table 5), Q_c and n -values are very often strongly correlated with the seismic activity and the fault density, in spite of high spatiotemporal variations of seismic activity (Figs. 2, 13) and long recurrence periods of large earthquakes in the Baikal rift (Chipizubov et al., 2009). The attenuation anisotropy of the lithosphere, associated with the formation of large-scale shear zones, is of special interest in our case study. Indeed, the anisotropy in shear zones results from the formation of schistosity and mylonite zones in the middle and upper crusts. In the uppermost part of the damaged zone, increased fracturing and rock crushing occur, leading to significant spatial heterogeneity of elastic properties along strike, expressed in the anisotropy of seismic waves. Attenuation of seismic waves is more sensitive to the anisotropy of the medium, as well as the grain size, than the velocity of seismic

waves (e.g. Tao and King, 1990; Carter and Kendall, 2006). The anisotropy in the shear zones of major faults of the SW Baikal rift (Main Sayan, Tunka, Obruchev and Primorsky faults) is clearly revealed by an increase of the attenuation coefficient across these large active faults by 20–60%. At the same time, the attenuation across fault zones is greater than along strike. Similar results have been obtained earlier by P-wave attenuation in the Khamar-Daban and Trans-Baikal regions (Dobrynina, 2011 and references therein). However, according to our results, it is not possible to distinguish among faults a degree of tectonic activity by using only the parameters of the anisotropy attenuation at this level of research.

5.5. Role of heat and fluids?

Active tectonic deformation and faulting processes, along with magmatism, play a key role in heat and fluid transport processes from depth to the surface. As pointed out Golubev (2007), convective heat transfer in groundwater is a major process determining heat flow in the Baikal rift system. Fluid saturation is known to increase attenuation of seismic waves (Romanowicz, 1994; Kopnichev and Sokolova, 2012). Along with the overall increase in fluid saturation in active regions, local variations related both to the structure of the lithosphere and to time-dependent internal processes are to be expected. For instance, pore-fluid pressure changes or fluid migration and related seismic attenuation are known to occur at short time scales in response to seismic strain build-up driven by stress loading during the seismic cycle, especially in pre- or post-seismic phases (Scholtz, 2002; Kopnichev and Sokolova, 2012; Rundle et al., 2013, and references therein). As discussed in the cases of regions of the Muya and North Lake Baikal, the increased heat flow likely affects the attenuation of seismic waves in these areas of active faulting and high seismic activity.

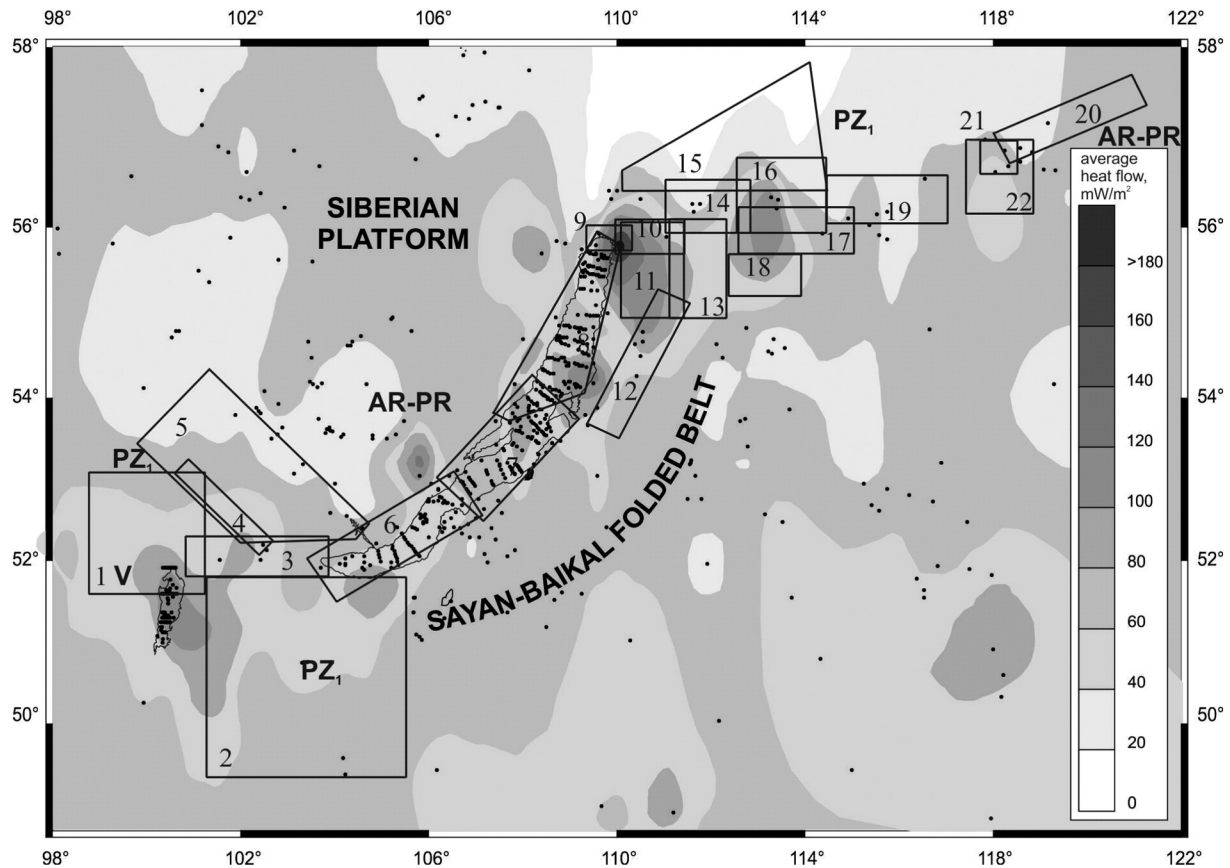


Fig. 15. Average heat flow (Duchkov, 1985; Golubev, 2000, 2007) and spatial distribution of Q_0 (Q -factor at frequency 1 Hz) and n frequency parameter: 1. Q_0/n ; 2. Points of heat flow measurement. We used a kriging interpolation algorithm to construct the map.

6. Conclusions

Using coda waves of 274 local earthquakes, a seismic quality-factor (Q_c), a frequency parameter (n) and an attenuation coefficient (δ) have been determined for the lithosphere of the Baikal rift and surroundings. We have determined the relationships between quality factor and frequency both at the scale of the whole area and of morphotectonic units (rift basins, uplifts, spurs, Siberian Platform, and Trans-Baikal belt). Using different lapse time windows (from 10 to 100 s with a step of 5 s), we compute the three attenuation parameters for different depths down to about 200 km. The comparison of these parameters with the velocity structures, seismic activity, surface fault density, heat flow and age/type of the crust led us to the following main conclusions:

- (1) Increase in the quality factor and decrease in the frequency parameter and attenuation coefficient with lapse time window (and accordingly depth) show that the upper part of the lithosphere is more heterogeneous compared to its lowest layers. Variations of attenuation parameters with depth are connected with the velocity structure of the region (especially the bottom of the Asian plate) while sharp changes in attenuation coefficient and frequency parameter coincide with velocity discontinuities.
- (2) Lateral variations of seismic wave attenuation correlate both with geological and geophysical characteristics of the Baikal rift system, showing that seismic wave attenuation depends primarily on seismic activity and heat flow of the region. The inherited geological heterogeneity of the medium and the age of the crust appear also to be important, although secondary, controlling factors.

- (3) Seismic wave attenuation in zones of main faults increases by more than 25–60% compared to neighboring areas. In these large shear zones (either of normal or strike-slip faulting types), anisotropy of the medium exerts a strong control on attenuation with a clear increased effect on waves traveling across the faults.
- (4) Faulting and active deformation increase thermal and fluid flow activity during rifting, leading to changes of the lithosphere properties, such as elastic modulus and anisotropy, which are reflected in attenuation.
- (5) Fluid-saturated lithosphere is characterized by lower viscosity, higher strain rates and, as a result, higher seismic activity and seismic wave attenuation (Romanowicz, 1994; Kopnichev and Sokolova, 2012). Time changes of pore-fluid pressure or fluid migration are indeed expected to occur at short time scales during the seismic cycle in response to seismic strain build-up within the upper crust of the Baikal rift system.

Finally, we stress that our results are dependent on the seismic station distribution: in our case study, most stations are located along the rift system (Fig. 3), while rift shoulders have still a poor data covering. Further studies aiming at collecting additional data in these areas are therefore needed in order to determine deeper and more resolved quality factor profiles.

7. Data and resources

Waveforms, catalogs and bulletins of earthquakes used in this study were collected by Baikal regional seismological center of Geophysical Survey of the Russian Academy of Sciences (<http://www.seis-bykl.ru>).

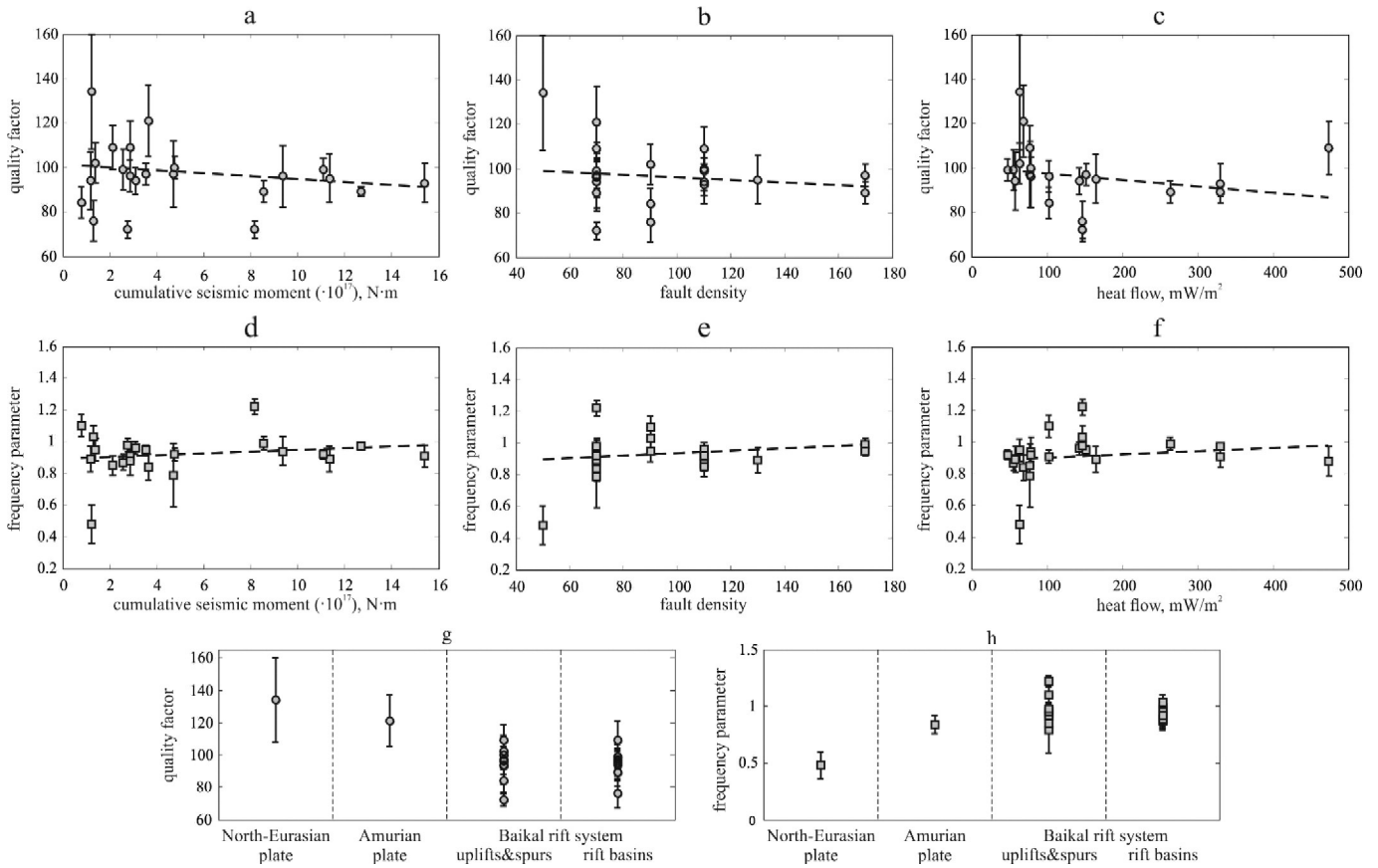


Fig. 16. Variations of quality factor Q_0 and frequency parameter n versus: (a,d) cumulative seismic moment, (b,e) surface fault density, and (c,f) heat flow, Bottom: distribution of the seismic Q -factor Q_0 (g) and frequency parameter n (h) for different tectonic structures: North-Eurasian and Amurian lithospheric plates and Baikalf rift.

Acknowledgments

The authors wish to thank Jean-Philippe Avouac and an anonymous reviewer for constructive comments and suggestions which improved this work. The authors wish to thank Carole Petit and an anonymous reviewer for constructive comments and suggestions which improved a previous version of this work. This study is carried out in the framework of a cooperation between Institute of the Earth’s Crust (Irkutsk) and Brest University. The reported study was funded by Russian Foundation for Basic Research (research project No. 13-05-01097_a), a joint project of Russian Foundation for Basic Research and Government of Irkutsk region (research project No. 14-45-04157_Siberia_a), by grant of the President of Russian Federation (research project No. MK 1171.2014.5).

References

Aki, K., 1969. Analysis of the seismic coda of local earthquakes as scattered waves. *J. Geophys. Res.* 74, 615–631.
 Aki, K., 1982. Scattering and attenuation. *Bull. Seismol. Soc. Am.* 72, S319–S330.
 Aki, K., Chouet, B., 1975. Origin of coda waves: source, attenuation and scattering effect. *J. Geophys. Res.* 80, 3322–3342.
 Anan’in, L.V., Mordvinova, V.V., Gots’, M.F., Kanao, M., Suvorov, V.D., Tat’kov, G.I., Tubanov, Ts.A., 2009. Velocity structure of the crust and upper mantle in the Baikalf rift zone from the long-term observations of broad-band seismic stations. *Dokl. Earth Sci.* 428 (7), 1067–1070.
 Aptikaeva, O.I., 1991. Frequency dependence and spatial and temporal variations in the quality factor from the records of frequency selective seismic stations and a modified Kirnos seismograph in the Garm test area. *Earthquakes and Processes of Their Preparation* (collected papers) (in Russian).
 Aptikaeva, O.I., Kopnichev, Yu.F., 1991. The fine structure of lithosphere and asthenosphere in the Garm region and its relationship with seismicity. *Dokl. Earth Sci. USSR.* 317 (2), 326–330 (in Russian).
 Bath, M., 1974. *Spectral Analysis in Geophysics*. Elsevier, Amsterdam (579 p).
 Calais, E., Vergnolle, M., San’kov, V., Lukhnev, A., Miroshnitchenko, A., Amarjargal, S., Déverchère, J., 2003. GPS measurements of crustal deformation in the Baikalf–Mongolia area (1994–2002: implications for current kinematics of Asia). *J. Geophys. Res.* 108 (B10), 2501. <http://dx.doi.org/10.1029/2002JB002373>.

Calvet, M., Sylvander, M., Margerin, L., Villaseñor, A., 2013. Spatial variations of seismic attenuation and heterogeneity in the Pyrenees: coda Q and peak delay time analysis. *Tectonophysics* 608, 428–439.
 Carter, A.J., Kendall, J.-M., 2006. Attenuation anisotropy and the relative frequency content of split shear waves. *Geophys. J. Int.* 165 (3), 865–874.
 Chipizubov, A.V., Smekalin, O.P., Semenov, R.M., Imaev, V.S., 2009. Paleoseismicity of cis-Baikalf region. *Probl. Eng. Seismol.* 36 (1), 7–22.
 Delvaux, D., Moyes, R., Stapel, G., Petit, C., Levi, K., Miroshnitchenko, A., Ruzhich, V., Sankov, V., 1997. Paleostress reconstruction and geodynamics of the Baikalf region, Central Asia. Part II: Cenozoic rifting. *Tectonophysics* 282, 1–38.
 Déverchère, J., Houdry, F., Diament, M., Solonenko, N.V., Solonenko, A.V., 1991. Evidence for a seismogenic upper mantle and lower crust in the Baikalf rift. *Geophys. Res. Lett.* 18 (6), 1099–1102.
 Déverchère, J., Houdry, F., Solonenko, N.V., Solonenko, A.V., Sankov, V.A., 1993. Seismicity, active faults and stress field of the North Muya region, Baikalf rift: new insights on the rheology of extended continental lithosphere. *J. Geophys. Res.* 98, 19895–19912.
 Dobrytnina, A.A., 2011. Coda-wave attenuation in the Baikalf rift system lithosphere. *Phys. Earth Planet. Inter.* 188, 121–126. <http://dx.doi.org/10.1016/j.pepi.2011.05.008>.
 Dobrytnina, A.A., Albaric, J., Deschamps, A., Perrot, J., Ferdinand, R.W., Déverchère, J., Sankov, V.A., Chechel’nitskii, V.V., 2012. Seismic waves attenuation in continental lithosphere under extensional condition: comparison of the East African and Baikalf rift systems. *Book of abstracts 33rd General Assembly of the European Seismological Commission (GA ESC 2012)*, 19–24 August 2012, Moscow and Young Seismologist Training Course (YSTC 2012), 25–30 August 2012, Obninsk – M., PH “Poligrafikwik”, pp. 32–33.
 Dobrytnina, A.A., Chechel’nitskii, V.V., San’kov, V.A., 2011. Seismic quality factor of the lithosphere of the southwestern flank of the Baikalf rift system. *Russ. Geol. Geophys.* 52 (5), 555–564. <http://dx.doi.org/10.1016/j.rgg.2011.04.008>.
 Dobrytnina, A.A., Chechel’nitskii, V.V., Sankov, V.A., 2014. *Quality factor of the Lithosphere and Source Parameters Baikalf Earthquakes – S-Peterburg: LAP LAMBERT Academic Publishing* 192 pp. (in Russian).
 Dobrytnina, A.A., 2013. Attenuation of seismic waves in the lithosphere of the northern part of the Basin and Range Province. *Geodyn. Tectonophysics* 4 (1), 53–67. <http://dx.doi.org/10.5800/GT2013410091>.
 Duchkov, A.D. (Ed.), 1985. *Catalog Data on Heat Flow in Siberia (1966–1984)* (Novosibirsk, 82 pp).
 Dutta, U., Biswas, N.N., Adams, D.A., Papageorgiou, A., 2004. Analysis of S-wave attenuation in south Central Alaska. *Bull. Seismol. Soc. Am.* 94, 16–28.
 Fagereng, A., 2013. Fault segmentation, deep rift earthquakes and crustal rheology: insights from the 2009 Karonga sequence and seismicity in the Rukwa–Malawi rift zone. *Tectonophysics* 601, 216–225.
 Gao, L.S., Lee, L.C., Biswas, N.N., Aki, K., 1983. Comparison of the effects between single and multiple scattering on coda waves for local earthquakes. *Bull. Seismol. Soc. Am.* 73, 377–389.

- Gao, S., Davis, P.M., Liu, H., Slack, P.D., Zorin, Yu.A., Mordvinova, V.V., Kozhevnikov, V.M., Meyer, R.P., 1994. Seismic anisotropy and mantle flow beneath the Baikal rift zone. *Nature* 371, 149–151.
- Golenetsky, S.I., Novomeiskaya, F.V., 1975. About earth crust's thickness from observation at Baikal seismic station network. In: Florensov, N.A. (Ed.), *Baikal Rift*. Nauka Publ. House, Siberian Branch, Novosibirsk, pp. 34–43 (in Russian).
- Golubev, V.A., 2000. Conductive and convective heat flow in the bottom of Lake Baikal and in the surrounding mountains. *Bull. Centres Rech. Explor. Prod. Elf-Aquitaine* 22, 323–340.
- Golubev, V.A., 2007. Conductive and Convective Heat Flow in the Baikal Rift Zone. Novosibirsk, Publ. house "Geo" (222 p).
- Gupta, S.C., Kumar, A., 2002. Seismic wave attenuation characteristics of three Indian regions: a comparative study. *Curr. Sci.* 82, 407–412.
- Gusev, A.A., 1995. Vertical profile of turbidity and Coda Q. *Geophys. J. Int.* 123, 665–672.
- Hasegawa, H.S., 1985. Attenuation of Lg waves in the Canadian shield. *Bull. Seismol. Soc. Am.* 75, 1569–1582.
- Havskov, J., Ottemoller, L., 2003. SEISAN: The Earthquake analysis Softwares for Windows, Solaris and Linux, Version 8.0. Institute of Solid Earth Physics, University of Bergen, Norway.
- Hazarika, D., Baruah, S., Gogoi, N.K., 2009. Attenuation of coda waves in the Northeastern Region of India. *J. Seismol.* 13, 141–160. <http://dx.doi.org/10.1007/s10950-008-9132-0>.
- Hellweg, M., Spudich, P., Fletcher, J.B., Baker, L.M., 1995. Stability of coda Q in the region of Parkfield, California: view from the U.S. geological survey parkfield dense seismograph array. *J. Geophys. Res.* 100, 2089–2102.
- Irandoust, M.A., Sobouti, F., Rahimi, H., 2016. Lateral and depth variations of coda Q in the Zagros region of Iran. *J. Seismol.* 20 (1), 197–211.
- Jolivet, M., Arzhannikov, S., Chauvet, A., Arzhannikova, A., Vassallo, R., Kulagina, N., Akulova, V., 2013. Accommodating large-scale intracontinental extension and compression in a single stress-field: a key example from the Baikal Rift System. *Gondwana Res.* 24, 918–935.
- Knopoff, L., Hudson, J.A., 1964. Transmission of love waves at a vertical discontinuity. *J. Geophys. Res.* 3969–3984.
- Kondorskaya, N.V., Shebalin, N.V. (Eds.), 1977. *New Catalog of Strong Earthquakes in the Territory of the USSR from the Earliest Times until 1975*. Nauka Publ. House, Moscow (in Russian).
- Kopnischev, Yu.F., Sokolova, I.N., 2012. Heterogeneities of the shear wave attenuation field in the lithosphere of East Tien Shan and their relationship with seismicity. *Dokl. Earth Sci.* 442 (Part 2), 292–295.
- Kopnischev, Yu.F., Sokolova, I.N., 2004. On the nature of an unusual wave train observed in the Northern Tien Shan region. *Bull. Seismol. Soc. Am.* 94, 1–5.
- Krylov, S.V., Mandelbaum, M.M., Mishen'kin, B.P., Mishen'kina, Z.P., Petric, G.V., Seleznev, V.C., 1981. *The Interior of Baikal From Seismic Data* (Nauka, Moscow, 105 pp., in Russian).
- Kvamme, L.B., Havskov, J., 1989. Q in Southern Norway. *Bull. Seismol. Soc. Am.* 79 (5), 1575–1588.
- Logatchev, N.A., 1993. History and geodynamics of the Lake Baikal rift in the context of the Eastern Siberia rift system: a review. *Bull. Centres Rech. Explor. Prod. Elf-Aquitaine* 17 (2), 353–370.
- Logatchev, N.A., Florensov, N.A., 1978. The Baikal system of rift valleys. *Tectonophysics* 45, 1–13.
- Lysak, S.V., 2002. Terrestrial heat flow in zones of active faults in southern east Siberia. *Russ. Geol. Geophys.* 43 (8), 791–803.
- Ma'hood, M., Hamzehloo, H., 2009. Estimation of coda wave attenuation in East Central Iran. *J. Seismol.* 13 (1), 125–139.
- Mak, S., Chan, L.S., Chandler, A.M., Koo, R., 2004. Coda Q estimates in the Hong Kong region. *J. Asian Earth Sci.* 24, 127–136.
- Mats, V.D., Ufimtsev, G.F., Mandel'baum, M.M., Alakshin, A.M., Pospeev, A.V., Shimaraev, M.N., Khlystov, O.M., 2001. *The Cenozoic of the Baikal Rift Valley: Structure and Geological History*. Nauka Publ. House, Siberian Branch, Novosibirsk 252 pp., in Russian.
- Matsumoto, S., Hasegawa, A., 1989. Two-dimensional coda Q structure beneath Tohoku, NE Japan. *Geophys. J. Int.* 99, 101–108.
- Mavko, G.T., Mukerji, G.T., Dvorkin, J., 2009. *The Rock Physics Handbook: Tools for Seismic Analysis of Porous Media*. Cambridge University Press.
- Mayor, J., Margerin, L., Calvet, M., 2014. Sensitivity of coda waves to spatial variations of absorption and scattering: radiative transfer theory and 2-D examples. *Geophys. J. Int.* 197 (2), 1117–1137. <http://dx.doi.org/10.1093/gji/ggu046>.
- Melnikova, V.I., Radziminovich, N.A., 2007. Parameters of seismotectonic deformations of the Earth's crust in the Baikal rift zone based on seismological data. *Dokl. Earth Sci.* 416, 1137–1139.
- Mitchell, B., 1981. Regional variation and frequency dependence of Q_b in the crust of the United States. *Bull. Seismol. Soc. Am.* 71, 1531–1538.
- Mohanty, W.K., Prakash, R., Suresh, G., Shukla, A.K., Walling, M.Y., Srivastava, J.P., 2009. Estimation of coda wave attenuation for the National Capital region, Delhi, India using local earthquakes. *Pure Appl. Geophys.* 166, 429–449. <http://dx.doi.org/10.1007/s00024-009-0448-7>.
- Mordvinova, V.V., 2009. The structure of the crust and upper mantle in Central Asia from the teleseismic body waves data. PhD thesis. Irkutsk. 35 p., in Russian. (unpublished).
- Mordvinova, V.V., Artyemyev, A.A., 2010. The three-dimensional shear velocity structure of lithosphere in the southern Baikal rift system and its surroundings. *Russ. Geol. Geophys.* 51, 694–707.
- Nikolaevsky, V.N., 1984. *Mechanics of the Porous and Fractured Media* (Moscow, Nedra. 232 pp., in Russian).
- Petit, C., Burov, E.V., Déverchère, J., 1997. On the structure and mechanical behavior of the extending lithosphere in the Baikal rift from gravity modeling. *Earth Planet. Sci. Lett.* 149, 29–42.
- Petit, C., Déverchère, J., 2006. Structure and evolution of the Baikal rift: a synthesis. *Geochem. Geophys. Geosyst.* 7, Q11016. <http://dx.doi.org/10.1029/2006GC001265>.
- Petit, C., Déverchère, J., Houdry, F., Sankov, V.A., Melnikova, V.I., Delvaux, D., 1996. Present-day stress field changes along the Baikal rift and tectonic implications. *Tectonics* 15, 1171–1191.
- Popov, A.M., 1990. A deep geophysical study in the Baikal region. *Pageoph* 134, 575–587.
- Pospeev, A.V., 2012. The velocity structure of the upper mantle and regional deep thermodynamics of the Baikal rift zone. *Geodyn. Tectonophysics* 3 (4), 377–383. <http://dx.doi.org/10.5800/GT-2012-3-4-0080>.
- Pujades, L., Canas, J.A., Egozcue, J.J., Puigvi, M.A., Pous, J., Gallart, J., Lana, X., Casas, A., 1991. Coda Q distribution in the Iberian Peninsula. *Geophys. J. Int.* 100, 285–301.
- Pullii, J.J., 1984. Attenuation of coda waves in New England. *Bull. Seismol. Soc. Am.* 74, 1149–1166.
- Radziminovich, N.A., Gileva, N.A., Melnikova, V.I., Ochkovskaya, M.G., 2013. Seismicity of the Baikal rift system from regional network observations. *J. Asian Earth Sci.* 62, 146–161.
- Radziminovich, N.A., 2010. Focal depths of earthquakes in the Baikal region: a review. *Izv. Phys. Solid Earth* 46 (3), 216–229. <http://dx.doi.org/10.1134/S1069351310030043>.
- Rautian, T.G., Khalaturin, V.I., 1978. The use of the coda for determination of the earthquake source spectrum. *Bull. Seismol. Soc. Am.* 68, 923–948.
- Roecker, S.W., Tucker, B., King, J., Hatfield, D., 1982. Estimates of Q in central Asia as a function of frequency and depth using the coda of locally recorded earthquakes. *Bull. Seismol. Soc. Am.* 72, 129–149.
- Rogozhina, V.A., Kozhevnikov, V.M., 1979. Anomal Mantle under the Baikal Rift. Nauka, Novosibirsk, pp. 1–104 (in Russian).
- Romanowicz, B., 1994. Anelastic tomography: a new perspective on upper-mantle thermal structure. *Earth Planet. Sci. Lett.* 128, 113–121.
- Rundle, J.B., Turcotte, D.L., Klein, W., 2013. *Geocomplexity and the physics of earthquakes*. Book Series: Geophysical Monograph Series <http://dx.doi.org/10.1029/GM120>.
- San'kov, V.A., Miroshnichenko, A.I., Levi, K.G., Lukhnev, A.V., Melnikov, A.I., Delvaux, D., 1997. Cenozoic stress field evolution in the Baikal rift zone. *Bull. Centres Rech. Explor. Prod. Elf-Aquitaine* 21 (2), 435–455.
- San'kov, V., Déverchère, J., Gaudemer, Y., Houdry, F., Filippov, A., 2000. Geometry and rate of faulting in the North Baikal rift, Siberia. *Tectonics* 19, 707–722.
- San'kov, V.A., Lukhnev, A.V., Miroshnichenko, A.I., Ashurkov, S.V., Byzov, L.M., Calais, E., Déverchère, J., 2009. Extension in the Baikal rift: Present-day kinematics of passive rifting. *Dokl. Earth Sci.* 425, 205–209.
- Sato, H., 1977. Single isotropic scattering model including wave conversions: simple theoretical model of the short period body wave propagations. *J. Phys. Earth* 25, 163–176.
- Sato, H., Fehler, M., 1998. *Seismic wave propagation and scattering in the heterogeneous earth?* Springer, Berlin (308 pp).
- Sato, H., Fehler, M.C., Maeda, T., 2012. *Seismic Wave Propagation and Scattering in the Heterogeneous Earth Vol. 496*. Springer-Verlag, New York.
- Scholtz, C., 2002. *The Mechanics of Earthquakes and Faulting*, second ed. Cambridge University Press, United Kingdom (471 pp).
- Sherman, S.I., Dneprovsky, Yu.I., 1989. *The Field Stresses of the Earth's Crust and the Geological-Structural Methods of Their Study*. Nauka Publ. House, Siberian Branch, Novosibirsk (in Russian).
- Sherman, S.I., 1978. Faults of the Baikal rift zone. *Tectonophysics* 45 (1), 31–40.
- Sherman, S.I., 1992. Faults and tectonic stresses of the Baikal rift zone. *Tectonophysics* 208, 297–307.
- Singh, S.K., Herrmann, R.B., 1983. Regionalization of crustal coda Q in the continental United States. *J. Geophys. Res.* 88, 527–538. <http://dx.doi.org/10.1029/JB088iB01p00527>.
- Solonenko, A., Solonenko, N., Melnikova, V., Shteiman, E., 1997. The seismicity and earthquake focal mechanisms of the Baikal rift zone. *Bull. Centre Rech. Elf Explor. Prod.* 21, 207–231.
- Suvorov, D.B., Tubanov, Ts.A., 2008. Distribution of sources of close earthquakes in the crust beneath the Central Baikal. *Russ. Geol. Geophys.* 49 (8), 611–620.
- Suvorov, V.D., Mishen'kina, Z.R., Petrick, G.V., Sheludko, I.F., Seleznev, V.S., Solovyev, V.M., 2002. Structure of the crust in Baikal rift zone and adjacent areas from deep seismic sounding data. *Tectonophysics* 354, 61–74.
- Tao, G., King, M.S., 1990. Shear-wave velocity and Q anisotropy in rocks: a laboratory study. *Int. J. Rock Mech. Min. Sci. Geomech. Abstr.* 27 (5), 353–361.
- Thybo, H., Nielsen, C.A., 2009. Magma-compensated crustal thinning in continental rift zones. *Nature* 457, 873–876. <http://dx.doi.org/10.1038/nature07688>.
- Tiberi, C., Diament, M., Déverchère, J., Petit, C., Mikhailov, V., Tikhotsky, S., Achauer, U., 2003. Deep structure of the Baikal rift zone revealed by joint inversion of gravity and seismology. *J. Geophys. Res.* 108 (B3), 2133. <http://dx.doi.org/10.1029/2002JB001880>.
- Zorin, Y.A., Mordvinova, V.V., Turutanov, E.K., Belichenko, V.G., Artyemyev, A.A., Kosarev, G.L., Gao, S.S., 2002. Low seismic velocity layers in the Earth's crust beneath Eastern Siberia (Russia and Central Mongolia: receiver function data and their possible geological implications). *Tectonophysics* 359, 307–327.